

ENHANCED ACTIVE TARGET DETECTION IN FOG

CENTRE FOR NEWFOUNDLAND STUDIES

---

**TOTAL OF 10 PAGES ONLY  
MAY BE XEROXED**

(Without Author's Permission)

ANDREW JOSEPH SMITH







## **INFORMATION TO USERS**

**This manuscript has been reproduced from the microfilm master. UMI films the text directly from the original or copy submitted. Thus, some thesis and dissertation copies are in typewriter face, while others may be from any type of computer printer.**

**The quality of this reproduction is dependent upon the quality of the copy submitted. Broken or indistinct print, colored or poor quality illustrations and photographs, print bleedthrough, substandard margins, and improper alignment can adversely affect reproduction.**

**In the unlikely event that the author did not send UMI a complete manuscript and there are missing pages, these will be noted. Also, if unauthorized copyright material had to be removed, a note will indicate the deletion.**

**Oversize materials (e.g., maps, drawings, charts) are reproduced by sectioning the original, beginning at the upper left-hand corner and continuing from left to right in equal sections with small overlaps.**

**Photographs included in the original manuscript have been reproduced xerographically in this copy. Higher quality 6" x 9" black and white photographic prints are available for any photographs or illustrations appearing in this copy for an additional charge. Contact UMI directly to order.**

**ProQuest Information and Learning  
300 North Zeeb Road, Ann Arbor, MI 48106-1346 USA  
800-521-0600**

**UMI<sup>®</sup>**

## **NOTE TO USERS**

**This reproduction is the best copy available.**

UMI<sup>®</sup>



**National Library  
of Canada**

**Acquisitions and  
Bibliographic Services**

**385 Wellington Street  
Ottawa ON K1A 0N4  
Canada**

**Bibliothèque nationale  
du Canada**

**Acquisitions et  
services bibliographiques**

**385, rue Wellington  
Ottawa ON K1A 0N4  
Canada**

*Your file Votre référence*

*Our file Notre référence*

**The author has granted a non-exclusive licence allowing the National Library of Canada to reproduce, loan, distribute or sell copies of this thesis in microform, paper or electronic formats.**

**The author retains ownership of the copyright in this thesis. Neither the thesis nor substantial extracts from it may be printed or otherwise reproduced without the author's permission.**

**L'auteur a accordé une licence non exclusive permettant à la Bibliothèque nationale du Canada de reproduire, prêter, distribuer ou vendre des copies de cette thèse sous la forme de microfiche/film, de reproduction sur papier ou sur format électronique.**

**L'auteur conserve la propriété du droit d'auteur qui protège cette thèse. Ni la thèse ni des extraits substantiels de celle-ci ne doivent être imprimés ou autrement reproduits sans son autorisation.**

**0-612-62426-9**

**Canada**

**ENHANCED ACTIVE TARGET DETECTION IN FOG**

by

© **ANDREW JOSEPH SMITH, B.ENG.**

**A thesis submitted to the  
School of Graduate Studies  
in partial fulfillment of the  
requirements for the degree of**

**MASTER OF ENGINEERING**

**Faculty of Engineering and Applied Science  
MEMORIAL UNIVERSITY OF NEWFOUNDLAND**

**November 2000**

**St. John's, Newfoundland**

***This thesis is dedicated to***

***Phyllis, Wayne, and Peter Smith***

***the most loving family (except brother) and hardest cases in the world***

# Abstract

Understanding and improving vision through fog and other scattering media has been a significant research area during the last century. Substantial knowledge has been gleaned from various scientific and engineering projects conducted in this period. Still, impaired vision due to fog wrecks havoc on the many forms of transportation that depend on vision as the primary source of navigation and guidance information.

This thesis details an investigation into the performance of several enhanced vision techniques, determining their advantages and disadvantages when imaging active targets through fog. To support this research, a low cost visibility sensor was designed to assist visual characterization of various marine advection fog events. This sensor was used during a series of field trials to evaluate the potential of visible and infrared technologies to enhance vision through fog. One system, polarization difference imaging, was found to have superior characteristics and could be used to improve visual guidance activities, such as helicopter operations on the Grand Banks, in degraded weather conditions. A design of a dedicated hardware, real-time target acquisition and tracking system based on polarization difference imaging suitable for enhanced guidance activities is proposed and discussed in detail. Ultimately, this research investigates the performance of several enhanced vision technologies in fog and proposes a solution that will improve offshore aviation in poor visibility conditions.

# Acknowledgements

I would like to extend my deepest gratitude to my graduate supervisors, Dr. Charles Randell and Dr. Raymond Gosine, for their time, encouragement, dedication, and support of my research activities. Dr. Randell has provided insight and guidance while helping me forge a path through piles of theory, ensuring that my work remained practical in nature. The successful completion of this thesis is in large part due to the kind words of Dr. Gosine. Dr. Gosine has provided inspiration, clairvoyance, and perspective to many the issues, both technical and not, that I have encountered during my graduate career. This work is a tribute to both of you.

I dedicate my sincere thanks to Desmond Power whose open door and technical expertise has been the key to creating many design solutions and understanding many technical issues throughout these past two years. Also, I must thank Faustina Hwang, Doug Pittman, and Jagan Seshadri, three of my fellow graduate students and friends who have understood the many general issues faced by graduate students and who have been great sounding boards for many of my wacky ideas.

As with everything in life, there are always people that provide support, humor, and friendship through one's journey through time and space. I would thank the following people: Richard Corbett, George Mann, Jamie King, Patricia Lefevre, Gerry Piercy, D'Arcy Hart, Parvez Kumar, Bob Robinson, Dave Reid, Peter Saturley, James Youden, Denny Christian, Don Guy, Dennis Johnson, Rod Hale, John Guzzwell,

**Gerry English, Jason Green, Karl Tuff, and all the staff at C-CORE.**

**I would like to thank the National Science and Engineering Research Council of Canada (NSERC) for funding my scholarship over the past two years, C-CORE for providing a fantastic technical environment and financial support, and the Faculty of Engineering and Applied Science for their financial and academic support.**

**Thanks to everyone for creating a fun-filled working environment and a most enjoyable two years.**

# Table of Contents

	<b>Page</b>
<b>ABSTRACT</b> . . . . .	<b>iv</b>
<b>ACKNOWLEDGEMENTS</b> . . . . .	<b>v</b>
<b>List of Terms and Abbreviations</b> . . . . .	<b>xii</b>
<b>Chapter 1</b>	
<b>1 Introduction</b> . . . . .	<b>1</b>
<b>1.1 Contributions of Thesis</b> . . . . .	<b>5</b>
<b>Chapter 2</b>	
<b>2 A Review of Enhanced Vision through Fog</b> . . . . .	<b>7</b>
<b>2.1 Fundamental Research</b> . . . . .	<b>8</b>
<b>2.2 Visibility Sensor Technology</b> . . . . .	<b>9</b>
<b>2.3 Visible Imaging and Image Enhancement</b> . . . . .	<b>11</b>
<b>2.4 Enhanced Vision Trends</b> . . . . .	<b>15</b>
<b>Chapter 3</b>	
<b>3 A Camera-Based Visibility Sensor</b> . . . . .	<b>21</b>
<b>3.1 Visibility Theory</b> . . . . .	<b>21</b>
<b>3.2 Camera Estimated Visibility</b> . . . . .	<b>24</b>
<b>3.2.1 Estimation Theory</b> . . . . .	<b>24</b>
<b>3.2.2 Sensor Calibration</b> . . . . .	<b>28</b>

3.3	Algorithm . . . . .	32
3.4	Results . . . . .	36
3.5	Recommendations . . . . .	40
<b>Chapter 4</b>		
4	Imaging of Active Targets Through Fog . . . . .	42
4.1	Experimental Setup . . . . .	43
4.1.1	Active Targets . . . . .	45
4.1.2	Enhanced Vision Systems . . . . .	49
4.2	Imaging Results . . . . .	54
4.2.1	Visible Imaging . . . . .	56
4.2.2	Polarization Difference Imaging . . . . .	60
4.2.3	Infrared Imaging (1-2.5 $\mu\text{m}$ ) . . . . .	63
4.2.4	Infrared Imaging (1-5.9 $\mu\text{m}$ ) . . . . .	66
4.2.5	Infrared Imaging (3-5 $\mu\text{m}$ ) . . . . .	67
4.2.6	Infrared Imaging (4-5 $\mu\text{m}$ ) . . . . .	69
4.3	Summary . . . . .	69
<b>Chapter 5</b>		
5	A Polarization Difference Imaging System . . . . .	71
5.1	Design Overview . . . . .	72
5.1.1	RS-170 . . . . .	73
5.2	PDI Design . . . . .	75
<b>Chapter 6</b>		
6	Concluding Remarks . . . . .	78
6.1	Future Work . . . . .	79
	REFERENCES . . . . .	81

# List of Tables

<b>3.1</b>	<b>Calculation of <math>C'_o</math></b>	<b>31</b>
<b>4.1</b>	<b>Weather Conditions</b>	<b>44</b>
<b>4.2</b>	<b>Day contrast measurements</b>	<b>57</b>
<b>4.3</b>	<b>Night contrast measurements</b>	<b>57</b>
<b>4.4</b>	<b>Normalized day contrast measurements</b>	<b>58</b>
<b>4.5</b>	<b>Normalized night contrast measurements</b>	<b>58</b>
<b>4.6</b>	<b>Visible target-background intensity measurements</b>	<b>59</b>
<b>4.7</b>	<b>PDI target-background intensity measurements</b>	<b>62</b>
<b>4.8</b>	<b>SWIR target-background intensity measurements</b>	<b>64</b>
<b>4.9</b>	<b>1-5.9<math>\mu</math>m target-background intensity measurements</b>	<b>66</b>
<b>4.10</b>	<b>3-5<math>\mu</math>m target-background intensity measurements</b>	<b>68</b>

# List of Figures

1.1	The Hibernia Gravity Based Structure . . . . .	2
1.2	Occurance of $< 1/2$ nm Visibility (Modified from [58]) . . . . .	4
3.1	Brightness Adaptation (Modified from [20]) . . . . .	26
3.2	Luminosity (Modified from [19]) . . . . .	27
3.3	Typical CCD sensitivity (Modified from [19]) . . . . .	28
3.4	Visibility estimation target . . . . .	29
3.5	Visibility: Belfort visibility sensors, February 23,2000 . . . . .	31
3.6	Visibility: Belfort visibility sensors, January 12,2000 . . . . .	32
3.7	Visibility estimation software interface . . . . .	33
3.8	Visibility estimation algorithm . . . . .	34
3.9	Target histogram in clear conditions . . . . .	35
3.10	Visibility: Belfort sensors, 9:21am-10:21am January 12, 2000 . . . . .	36
3.11	Visibility: Belfort sensors, 11:07am-12:07pm January 12, 2000 . . . . .	37
3.12	Visibility: Image Processing Algorithm using Equation 3.3. . . . .	38
3.13	Visibility: Image Processing Algorithm using Equation 3.2. . . . .	39
3.14	Visibility: Image Processing Algorithm using Equation 3.2. . . . .	40
4.1	Blackbody approximations of a 3000W element and a QH source . . . . .	46
4.2	Transmission Spectra for Soda-Lime Glass . . . . .	47

4.3	Active targets in the 4-5 $\mu\text{m}$ region under clear conditions . . . . .	48
4.4	Active targets in the 3-5 $\mu\text{m}$ region under clear conditions . . . . .	49
4.5	The 500W QH source in the 1-2.5 $\mu\text{m}$ region under clear weather conditions . . . . .	50
4.6	The concept of polarization difference imaging . . . . .	51
4.7	Long-IR imaging under clear weather conditions . . . . .	53
4.8	Atmospheric transmission windows . . . . .	55
4.9	Visible image of active targets: Day visibility 0.250-0.350 km . . . . .	60
4.10	Visible image of active targets: Night visibility 0.300-0.400 km . . . . .	61
4.11	Horizontal, vertical, and polarization difference images: Daytime visibility 0.250-0.350km . . . . .	63
4.12	SWIR image of the targets under nighttime fog conditions . . . . .	65
4.13	1-5.9 $\mu\text{m}$ image of the targets under moderate daytime fog conditions . . . . .	67
4.14	3-5 $\mu\text{m}$ images of the targets under moderate daytime fog conditions . . . . .	68
5.1	Physical setup of the PDI system . . . . .	72
5.2	Timing diagram of the RS-170 waveform (Modified from [57]) . . . . .	74
5.3	Circuit design of the PDI target acquisition and tracking system . . . . .	75
5.4	Sample vertical and horizontal signals . . . . .	76

# List of Terms and Abbreviations

<b>ALBEDOS</b>	<b>Airborne Laser Based Enhanced Detection and Observation System</b>
<b>CCD</b>	<b>Charge Coupled Device</b>
<b>COAR</b>	<b>Consortium for Offshore Aviation Research</b>
<b>C-CORE</b>	<b>Center for Cold Oceans Resources Engineering</b>
<b>DERA</b>	<b>Defence Evaluation and Research Agency</b>
<b>DREV</b>	<b>Defense Research Establishment Valcartier</b>
<b>EIA</b>	<b>Electronics Industry Association</b>
<b>EV</b>	<b>Enhanced Vision</b>
<b>FASCOD</b>	<b>Fast Atmospheric Signature Code</b>
<b>GBS</b>	<b>Gravity Based Structure</b>
<b>GPS</b>	<b>Global Positioning System</b>
<b>HUD</b>	<b>Heads-Up Display</b>
<b>HiTran</b>	<b>High Resolution Transmittance Code</b>
<b>IR</b>	<b>Infrared</b>
<b>LowTran</b>	<b>Low Resolution Transmittance Code</b>
<b>MMW</b>	<b>Millimeter-Wave</b>
<b>ModTran</b>	<b>Moderate Resolution Transmittance Code</b>
<b>MTF</b>	<b>Modulation Transfer Function</b>
<b>MWIR</b>	<b>Mid-Wave Infrared</b>

<b>OD</b>	<b>Optical Depth</b>
<b>PDI</b>	<b>Polarization Difference Imaging</b>
<b>PMMW</b>	<b>Passive Millimeter-Wave</b>
<b>PSF</b>	<b>Point Spread Function</b>
<b>ROI</b>	<b>Region Of Interest</b>
<b>QH</b>	<b>Quartz-Halogen</b>
<b>SWIR</b>	<b>Short-Wave Infrared</b>

# Chapter 1

## Introduction

*Half-steam ahead, by guess and lead, for the sun is mostly veiled—  
Through fog to fog, by luck and log, sail you as Bering sailed...*

Rudyard Kipling, *The Seven Seas*

Since the beginning, man has aspired to climb the highest mountain, dive beneath the deepest sea, and trek to the far reaches of the earth in search of fame, knowledge, and wealth. Throughout his journey through time and space, man has traveled with nature, a companion whose power is unrivaled by any creature on this planet. From Robert E. Peary's and Matthew Henson's trek to the North Pole to Sir Edmund Hillary's and Tenzing Norgay's climb of Mount Everest; from John Cabot's exploration of the new world to Yuri Gagarin's maiden voyage into the vastness of space, nature has been ever-present, constantly placing new challenges and obstacles in an attempt to impede man's epic journey.

Man's quest for knowledge and understanding requires the development of new technologies which, in turn, place increased demands on the earth's natural resources. The increased demand for natural resources requires that these resources be extracted



Figure 1.1: The Hibernia Gravity Based Structure

from many of the most inhospitable environments in the world. These harsh environments place significant demands on the technology and operators working in these settings, resulting in an increased risk to the environment and to human life. Additional technologies must be designed to assist operation in these environments, reducing risk and improving efficiency.

One harsh environment that has recently become the center of activity is located on the Grand Banks of Newfoundland. In December 1997, Hibernia, a gravity-based oil production platform, started production 315 km off the East Coast of Newfoundland. The structure has an estimated field life of 18 years with an average daily plateau production rate of 135,000 barrels per day for the next 6 years [3]. Figure 1.1 shows the Hibernia GBS under clear weather conditions.

The north eastern Atlantic is also well known for the dense fog, high winds, severe storms and drift ice that combine to form one of the worlds most hostile operating environments. In fact, the Grand Banks is noted as the foggiest place in the world by the Guinness Book of Records [4]. Dense advection fogs form when the warm, humid air from the south meets the cold waters of the Labrador current. Occasionally, the fog has been noted so thick that it becomes unsafe to operate cranes [5]. Statistics gathered by ships over the last century indicate the peak fog months and their frequency of occurrence on the Grand Banks. These results are shown in figure 1.2. The fog, along with the other environmental hazards, makes the Grand Banks a very difficult working environment and introduces significant risks to the operators and their constructs.

The transportation of workers to offshore structures in Canada, such as Hibernia, is regulated by Transport Canada. The regulations are strictly enforced to minimize the transportation risks that commuters face while traveling to and from these offshore facilities. The current laws regarding these flights state the approach minima as being  $\frac{1}{2}$  nautical mile and 280' above mean sea level [6]. The pilot cannot begin his approach unless he has visual confirmation of the landing area outside the approach minima. These regulations reduce risk to commuters by forcing the pilot to execute a missed approach far from the rig, allowing time to perform the necessary maneuvers.

The major hazards associated with operating under reduced visibility conditions is the lack of situational awareness. Thick fogs reduce the visual contrast of the surrounding environment, obscuring obstacles, forcing operators to make decisions based on incomplete information. Advanced sensor systems provide additional situational information, such as altitude, location, and enhanced scenery, permitting the pilot to make more informed decisions. Global Positioning Systems (GPS), heads-up displays (HUDs), thermal imagers, and millimeter wave imagers are several of the key technologies used to increase a pilots situational awareness.

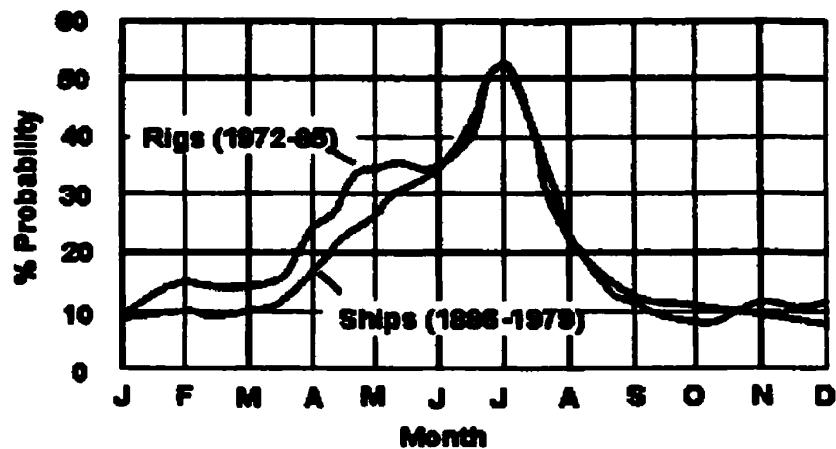


Figure 1.2: Occurance of < 1/2 nm Visibility (Modified from [58])

Lack of offshore aviation research, coupled with the strict regulatory process, has so far prevented the use of these technologies to change the current approach regulations. In time, however, many of these technologies will be incorporated into offshore aviation operation and will be deemed acceptable additions to flight operations. The actual process of dealing with the regulatory hurdles is a complex issue and is beyond the scope of this work.

## **1.1 Contributions of Thesis**

In early 1998, three high intensity searchlights were installed on the helideck of the Hibernia GBS. A joint study performed by C-CORE and DREV (Defence Research Establishment Valcartier) proposed that a visible lighting system would provide the helicopter pilots with a reliable visual reference to assist a successful landing [36, 16]. Motivated by the results of this study, this thesis investigates the potential of several enhanced vision techniques aimed at improving a pilot's ability to detect these types of searchlights or other active targets under inclement weather conditions.

A detailed review of the literature has been completed and presented in Chapter 2. This review discusses many of the technologies and approaches, being examined by the scientific community, that focus on improving situational awareness under poor visibility conditions.

A novel camera-based visibility estimation system has been designed and tested under extreme Newfoundland weather conditions. The underlying algorithm has been designed using fundamental visibility theory developed throughout this century. Comparisons between this system and commercial off-the-shelf visibility sensors show that this system performs quite well under various fog conditions. The algorithm, sensor design, and test results are presented in Chapter 3.

One of the main contributions of this work is the field trials investigating the ability of various vision sensors to image active targets through marine fog. This study uses the visibility sensor described in Chapter 3 along with several other weather measurements to help characterize the vision sensor performance. Several infrared and visible imaging solutions are examined to determine if these systems offer any improvement to offshore aviation and other operations in poor visibility conditions. This is one of the premier studies of enhanced vision through marine advection fog and supports the findings of several other trials investigating enhanced vision performance

in fog. One key conclusion determined during this work suggests that Polarization Difference Imaging would be an excellent supplement to current guidance and navigation information. The details and results of the field trials are presented in Chapter 4.

A simple hardware implementation of the Polarization Difference Imaging system is proposed in Chapter 5. This chapter details the high level design of a compact, lightweight system that will enhance navigation and guidance under poor visibility conditions. Implementation and testing of this system is left for future work.

Chapter 6 contains a summary and discussion of the future work that will further research in the field of offshore aviation. This thesis provides an initial step in developing research expertise in aviation operations on the Grand Banks and provides direction for future work in this area.

## **Chapter 2**

# **A Review of Enhanced Vision through Fog**

**Visibility and research topics associated with vision through the atmosphere has been an active research area for the past three centuries. Much of the research towards definitions and governing equations, along with investigations detailing the propagation of light through fog, has taken place during the first half of the twentieth century. Enhanced vision, any technique that improves human vision, is a much more recent topic that has seen extensive work from the 1960's onwards. Early research in this area has been conducted by the military and was generally classified. As time passed, these technologies started to find a place in commercial industry, resulting in increased research activity adapting these enhanced vision technologies to many diverse applications.**

**This chapter represents a review of the literature, providing the reader with insight into the key works that set the stage for enhanced vision and visibility research. The discussion begins in the mid-1700's and progress to the state-of-the-art technologies being developed today. It should be understood that there is a considerable amount**

of literature available on this very broad topic and only work that has bearing on this research is included in the review. The review will bring the reader to the forefront of current trends in enhanced vision and visibility research.

## 2.1 Fundamental Research

During the latter part of the 18<sup>th</sup> century, Bouger, a French researcher, presented a short chapter on the transparency of the atmosphere. This work was followed by Lord Rayleigh in the 19<sup>th</sup> century, who dealt quite extensively with the scattering of light by air and by other small spherical particles [2]. These two works built a foundation of knowledge for research into the visibility of objects that proceeded during the early 20<sup>th</sup> century.

In 1924, Koschmieder presented his work on the visual range of objects under various atmospheric conditions [9]. He presented the exponential decaying relationship that exists between the extinction coefficient and the apparent contrast of objects, a topic discussed in detail in Chapter 3. The research by Koschmieder is fundamental background theory for most research regarding visibility and vision through the atmosphere.

Research into imaging through the atmosphere increased dramatically during the war years leading to the development of sensors capable of estimating the extinction coefficient and, hence, the visual range. Most of the accepted theories and additional research completed during this period was bound in a comprehensive book by W. E. Middleton titled *Vision Through The Atmosphere* [2]. The theories presented in this publication, considered by many to be the 'bible' of vision through the atmosphere, remain as important today as they were when the book was published back in 1952.

From the 1950's onwards, there has been an increased interest in understanding and modeling the propagation of electromagnetic energy through the atmosphere. In

1965, the Air Force Cambridge Research Laboratories published the book *Handbook of Geophysics and Space Environments*, a collection of data, formulae, definitions, and theories about the earth's environment [21]. Included in this book are several chapters dealing with atmospheric optics and the transmittance of electromagnetic waves through the atmosphere. This publication is based mainly on experimental data and indicates many of the transmission windows and absorption bands present in the atmosphere.

The development of the transistor and advanced computing systems assisted the development of computer models of the atmosphere. These models are capable of predicting the wavelength-dependent attenuation of electromagnetic wave propagation through particular atmospheric conditions. FASCOD, a software package developed during the early 80's, is one example of an atmospheric modelling package. FASCOD was designed to calculate the radiance and transmittance of a medium with specific applicability to the earth's atmosphere [22]. The program predicts the impact on wavelengths, from the visible to the microwave region, due to the seven principal absorbers in the atmosphere. Other popular models include LowTran, ModTran, and HiTran, each having their own specific characteristics.

The research conducted from the 1700's to the early 1980's provided the foundation for the development of advanced visibility sensors and enhanced vision technologies. The next couple of sections examine state of the art developments in visibility estimation and enhanced vision technologies in the visible to millimeter-wave regions.

## 2.2 Visibility Sensor Technology

This section details many of the current trends in visibility estimation systems. Some of the older technologies are presented briefly with the main focus on the more recent and currently used technologies.

The development of sensors capable of estimating the visibility has come a long way since the design of original transmissometers nearly half a century ago. These sensors generally measured the extinction of light over an optical path of approximately 250'. The extinction coefficient is related to the visibility via a mathematical relationship discussed in Chapter 3. These devices are relatively expensive to install and generally require frequent maintenance and calibration.

In the early 1980's, Edward Spitzer proposed that it was possible to estimate the extinction coefficient by measuring the amount of forward-scattered light [23]. These sensors, known as forward-scatter sensors, have been extensively tested to determine their reliability in estimating the visibility. An active source and detector are mounted at close range and at specific angles with respect to the horizon and each other. A publication by Tonna and Shifrin in 1992 supported the idea that these sensors accurately estimate visibility [10]. They state that visibility can be accurately estimated using a source ranging from  $0.25\mu\text{m}$  to  $1.06\mu\text{m}$ , depending on the angle between the source and detector. The forward-scatter visibility sensors have typically been employed, with increasing frequency, at airports and along roadways that experience frequent poor visibility conditions. In 1994, a simple forward-scatter sensor design was published by Mill [11].

As science and technology advanced, other estimation methods were designed for many diverse applications. In 1995, Bendix proposed an algorithm for estimating the visibility using a high-resolution radiometer operating aboard an environmental satellite [12]. This concept can be used in many applications including remote environments where measurement sensors are not available. Another area receiving increased attention is visibility estimation from a moving vehicle. Two different methods of estimating the visibility from a highway vehicle were published in 1998. Pomerleau described a method that measured the contrast of consistent road features such as the lane markings and road shoulders [13]. The visibility was correlated to the location

of particular contrast levels within the scene. Busch relied on the wavelet transform and various edge detection techniques, instead of direct contrast measurement, to estimate the visibility [14]. The key concept in this work relied on the fact that sharp, well-defined edges usually correlate with high contrast areas. One again, this method was correlated with a measure of the visibility.

As imaging sensors and computational technology becomes faster and less expensive, these concepts will begin to see greater acceptance in many commercial applications. While these papers indicate current trends in visibility research, a discussion of visibility and the theory in Chapter 3 provides the necessary background for the development of a new visibility estimation system using a simple camera-target setup.

## **2.3 Visible Imaging and Image Enhancement**

Image propagation through fog, along with research in image enhancements pertaining to aviation, visible imaging techniques and visual flight aids all add value to the offshore aviation industry in Newfoundland. These topics are presented in this section, providing the reader with an overview of scientific trends and developments in visible imaging and image enhancement through fog.

The area of image propagation through a scattering medium is an extensively studied area with many models and theories having been developed to explain the associated phenomena. It is understood that the propagation of electromagnetic waves through fog is dependent on the droplet size distribution. Some wavelengths may have better penetration abilities than others depending on the specific conditions of a fog event. When examining the visible spectrum, all wavelengths are generally attenuated equally by a fog. Specific wavelength advantages do come into play when an active source is carefully matched with a detector's peak sensitivity, hence the reason for orange lights on automobiles. In 1984, Kopeika defined a relationship between

the atmospheric Modulation Transfer Function (MTF) and the particle size distribution, stating that this relationship plays a strong role in the wavelength dependence of imaging through the atmosphere [24]. Knowledge of the size distribution, along with other characteristics of the fog event, can lead to predictions of the best spectral region for imaging through various fogs.

The work of Kopeika was followed by Bissonnette, in 1990, who completed a series of research projects investigating imaging through rain and fog. First, Bissonnette described a method for calculation of the MTF in an aerosol media [25]. The calculation method exhibited good consistency when compared to actual measurements. A systematic validation of the measurement was completed in 1991 when Bissonnette conducted a series of tests to determine the Point Spread Function (PSF), related to the MTF by a 2-dimensional Fourier Transform, and the blurring effects of fogs [26]. The test results supported the calculated MTF models. One conclusion of this work indicated that aerosol blurring effects were negligible for most fogs. Significant blurring was present for rain and some advection fogs with particle sizes in the range of  $100\mu\text{m}$ . In 1992, a concluding paper by Bissonnette described brightness and contrast reduction as a function of scattering losses due to fog events [27]. Linskens and Bohren supported some of Bissonnette's predictions with their 1994 paper on the appearance of the sun and moon as seen through in clouds [28]. Linskens and Bohren found that the sun's disk could be seen through the atmosphere when the optical depth was less than 10 and that blurring would occur when the atmosphere contained a significant number of large particles at moderate optical depths. The contributions of these authors provide an extensive investigation into the impact of rain and fog on an imaged scene.

Recently, there have been a number of papers published on image enhancement in fog, specifically for aviation applications. A paper by Oakley, published in 1996, dealt with the enhancement of images from a forward-looking airborne camera [29].

Oakley claimed that the typical contrast enhancements used in image processing does not significantly increase the visibility in a murky image. He used this reason to warrant the development of a new algorithm focused on increasing the visibility in images. This new algorithm estimated the percent scattered light and the percent direct light incident on each pixel in the imaging sensor. The percent weighting for each pixel is dependent on range information. A temporal filter was employed, in conjunction with the above algorithm, to reduce the impact of sensor noise and improve the overall image quality. Oakley and Satherly published a second paper in 1998 that described the details of their algorithm. The algorithm used a physical model for the contrast degradation based on the theories of Kopeika, Bissonnette, and others [30]. Experimental results indicated that the algorithm worked well for haze and that it should work well for fog and cloud conditions. No testing has been completed under fog and cloud conditions to date. The authors state that the image quality is significantly improved over traditional contrast enhancements and that real-time testing of this system over a wider range of conditions is planned for the future.

An alternate imaging method used to enhance detectability of specific objects through a scattering medium was investigated in 1997. Engheta and Tyo investigated the use of polarization difference imaging (PDI) to enhance object contrast. [31]. The idea was inspired by creatures that use light polarizations as a means to enhance vision in highly scattering media such as underwater. Tyo, in his doctoral thesis, described the method of PDI and the investigations that provided insight into this imaging method [32]. Tyo's work involved the difference imaging of specially designed polarized targets immersed in a milk and water solution. PDI is examined in chapter 4 and 5, along with several other imaging techniques, each focused on the imaging of an active target in fog conditions.

The discussion now focuses on various flight aids designed to improve offshore flight operations. One such aide is a laser approach system, designed by Laserline

Corp., used for night approaches of fixed wing military aircraft on approach to aircraft carriers. The pilot must fly directly into the beam of this eye-safe laser lighting system, adjusting his approach to the carrier based on the color and flash-rate of the incident light [33]. Cougar helicopters conducted a series of trials in 1997 investigating the potential of this system to assist approaches to offshore oil structures [34]. Tests indicated that the system assisted approaches in both day and night conditions but that additional testing was required to understand the performance in restricted visibility conditions. It was noted that the major obstacle facing this approach system would be of a regulatory nature. Transport Canada, the regulatory body, has no regulations regarding this type of approach. Significant resources would be required to develop an approach using this technology with no guarantee that it would reduce the existing approach minima.

DERA, a research organization located in the UK, has spent considerable resources investigating different approach technologies directed at improving offshore aviation. This group published a review of their investigations at the 1998 Consortium for Offshore Aviation Research (COAR) meeting [35]. In this report, DERA discusses their investigations into the use of high intensity lights mounted on the edge of the landing area, with particular interest of improving night flights. Their findings indicated that the lights were unsatisfactory due to glare and relatively high ambient light levels related to the presence of many offshore rigs. Detailed investigations into advantages searchlights provide under daytime fog conditions were not conducted.

In 1996, Bissonnette developed a model that predicted the detection range of a searchlight as a function of visibility and searchlight photopic radiance [36]. Simulations indicated that a searchlight would be detected at a range approximately three times greater than the current daytime visibility in optical depths greater than 10. The model was verified at the Defence Research Establishment Valcartier's (DREV) aerosol test facility in Quebec, Canada. Experimental results supported the models

predictions but found that searchlights were seen at a range greater than the model predicted. This was attributed to the lack of scattered light from the sun, a very significant factor, that would normally obscure the observer's vision. Bissonnette suggested that testing should occur in natural daytime fog conditions to further support the accuracy of this model. In support of Bissonnette's conclusions C-CORE, a research and development company based in Newfoundland, continued the investigation of high powered searchlights as a approach aid in daytime fog conditions. Hart and Piercey conducted preliminary investigations into the effectiveness of searchlights in fog, recording baseline data under clear conditions [37]. Additional research in "real world" conditions is required to support the Bissonnette model's predictions.

## **2.4 Enhanced Vision Trends**

Enhanced vision is viable solution that will improve aviation in poor visibility conditions. The development of an all-weather penetrating imaging system has been goal of many researchers worldwide. Extensive research in this area began with the military in the 1960's and has continued to garner attention in commercial industry today. Infrared, millimeter-wave, and range-gated laser imaging are just some of the technologies that seek acceptance as a supplement that will enhance vision through fog. These systems, each with their advantages and disadvantages, have undergone significant testing in recent years that characterize their performance under foggy conditions. A review of enhanced vision technologies and current research trends is presented in this section with the main emphasis on enhanced vision through fog.

High-level design and stringent specification of enhanced vision systems has provided research with direction and support necessary to guide this rapidly advancing field. Several papers have identified many of the fundamental objectives of an enhanced vision system designed for the civilian aviation industry. Larimer, in 1992,

specified the three main criteria for a system designed to "see" through the fog as being guidance, hazard detection and hazard recognition [38]. He commented on the two primary enhanced vision technologies, infrared and millimeter-wave imagers, stating that infrared imaging systems typically have good spatial resolution but poor weather penetrating ability whereas the millimeter-wave imagers have excellent weather penetration but poor spatial resolution. This is a commonly understood and accepted statement within the enhanced vision industry. Larimer indicated that the optimal enhanced vision solution will stem from the fusion of the two imaging systems.

The concepts identified by Larimer are supported in publications by NASA in 1993 and Kaiser in 1994 [39] [40]. Kaiser points out that the key difference between military and commercial aviation applications is the level of acceptable risk. Civilian aircraft have a very low tolerance of risk, much lower than military aircraft. Another major difference between the military and civil aviation is that solutions for the latter must be cost-effective and add value to the company due to the competitive nature of commercial flight.

Sweet augmented the knowledge of high-level sensor performance issues with her 1996 paper and supported the idea that sensor fusion between millimeter-wave and infrared systems would typically provide the optimal enhanced vision solution [41]. Sweet discussed some issues related to the image fusion and image registration, a key component of fusion. The general trend towards sensor fusion is supported in a 1997 article on FLIR Systems' approach to the fusion concept [42]. As other groups research the fusion of multiple sensor inputs, the idea of an all-weather penetrating aviation solution is near becoming a reality. Next, some of the specific sensor solutions that have sought to improve vision through fog and other poor weather conditions are examined.

Infrared (IR) imaging has long been thought of as the key to imaging through fog though many field trials have indicated otherwise. The automotive industry has

been interested in the use of IR systems as a night-time driving aid and also as an enhancement to vision in poor visibility conditions. To characterize the performance of these systems under foggy conditions, several groups have conducted extensive studies under a wide variety of meteorological conditions.

In 1994, Beier et al. conducted an extensive study of IR sensors and their potential as an enhanced vision aid for driving in foggy conditions [43]. This study included the modeling of IR propagation using LowTran, the measurement of fog characteristics such as visibility and droplet size spectra, and a series of field trials involving many different imaging sensors with both passive and active targets. There were a number of major conclusions drawn from this project dealing with IR imaging through fog from an automotive perspective. First, Beier commented that an increased visibility in the IR could be achieved by matching the peak-emissivity of an active target with the peak-detectivity of the imaging system. This is key if the imaging system is designed to image the IR signature of special car headlights better than the human eye. Second, the IR spectral range is not as good as visible in rain or snow. Finally, only in special cases such as light fog or haze, is the IR visibility better than the visible.

A thorough review of vision enhancement technologies was compiled by Denes in 1995 [44]. This included a summary of both military and commercial research completed at the time of publication. One major discovery by the military found that there are two types of fogs, wet and dry. Under dry fog conditions, IR imaging systems provided a substantial improvement over visible imaging systems. Under conditions with 250m visibility, IR visibilities of 2 km were measured. Under wet fog conditions, both visible and IR images were similarly degraded. This illustrates the dependence of IR imaging on the liquid water content of the optical path. In his review, Denes described many different types of detector materials and imaging systems, providing a summary of the current trends in IR imaging. This review

quickly brings the reader up to speed with current infrared enhanced vision research.

A paper presented by Lane in 1995 examined the benefits of imaging in the short-wave region as opposed to the visible and near IR regions [45]. At long ranges and under low visibility conditions, the signal-to-noise ratio and image quality was superior in both theory and experimental evidence.

In 1998, another investigation was conducted that evaluated the use of thermal imagers as an automotive enhanced vision system. The experiment completed by MacCarley was less extensive than Beier's experiment but did attempt to examine the use of IR cameras in fog [46]. During the experiment, MacCarley tested a series of IR cameras under nighttime and light fog conditions. Very little testing was completed in dense fog conditions. Results of the experiment under light fog conditions indicated that the IR cameras provided good surveillance capability but only comparable to visible imaging.

In general, experimental evidence has shown that thermal imaging systems provide little or no advantage to imaging through fog. Testing carried out by independent groups have indicated that the imaging of passive targets is equal to or worse than that of standard visible imaging. The potential of IR systems to image active targets, under dense marine fog conditions, is examined in Chapter 4 to validate and expand the findings in these studies.

Significant resources have been focused on the development of millimeter-wave (MMW) imaging systems. These systems have excellent fog penetration abilities, due to the low attenuation of long wavelengths, but have relatively poor spatial resolution. The poor spatial resolution limits their effectiveness as an independent enhanced vision technology but, when combined with other imagers and fusion techniques, may provide a solution to reducing weather related delays at airports. In 1992, Horne discussed the results of several flight trials conducted using an active MMW imaging sensor [47]. The MMW image was not noticeably degraded by low ceilings

or other poor visibility conditions. This work was followed by Bradley in 1993 who stated that MMW systems currently had the ability to image airports and their surrounding environment in poor meteorological conditions [48]. The area of MMW imaging has seen some major companies promote and develop various types of MMW imaging sensors. In 1994, Thermotrex announced that they had developed an imaging radiometer for aviation application [49], further adding to the momentum of MMW research.

In the early 1990's, the research focus of MMW imagers diverged into several paths. Work continued on the imaging radiometers but a major emphasis was placed on the development of a Passive Millimeter-Wave (PMMW) Camera. In 1995, Shoucri presented some of the advances PMMW imaging has made over the last couple of years that has facilitated the development of a manufacturable economic camera [50]. This camera, as presented by Yujiri in 1997, operates at 89 GHz, is capable of real time imaging, and has a focal plane array consisting of 1024 pixels [51]. Fornaca, in 1998, discussed some of the flight tests and stated that the camera gave excellent all-weather penetrating ability [52]. The current focus remains on the optimization and further flight testing of this system.

Another technology currently being investigated as an enhanced vision tool is a laser-based, range-gated active imaging system using an eye-safe laser as the active source. Bonnier and Larochelle, associated with DREV in Canada, presented a series of papers on the development of ALBEDOS, Airborne Laser Based Enhanced Detection and Observation System [53] [54]. Generally, Bonnier and Larochelle found that this system had better fog penetration capabilities, especially when the targets had retroreflective properties, and had better imaging resolution than thermal imagers. The major drawback to this system was the fact that the laser energy had to propagate twice the distance as that of other passive imaging systems. Additional field trials under a broad range of conditions are planned for the future.

**There are many technologies designed to improve and enhance vision through fog spanning from visible imaging to millimeter-wave imaging. Each system has advantages and disadvantages with respect to their imaging performance and the specific details of their application. Until the time when these sensor systems become sophisticated enough to permit flight in zero visibility conditions, science will continue work in the area of enhanced vision systems.**

# Chapter 3

## A Camera-Based Visibility Sensor

This chapter describes the design and development of a camera-based visibility estimation system. Visibility is one of the fundamental features of a fog event and its measurement is key to evaluating imaging system performance under these conditions. This sensor system is constructed using a simple black and white target in combination with a video camera. The contrast of the black and white target is measured and the visibility is calculated based on established theoretical relationships. In support of the validity of the camera-target system, a discussion of visibility and its relationship to contrast is presented.

### 3.1 Visibility Theory

The term visibility, in reference to daytime viewing conditions, has taken on a number of meanings over the years. According to Huschke, daytime visibility is the greatest distance at which an observer can discern a prominent dark object from its background with the unaided eye [1]. This term is rather subjective, as it is observer-dependent, and has led the scientific community to produce more definitive terms.

In Middleton's treatise, *Vision Through The Atmosphere*, the visual range is de-

defined as the range at which an object of definite size and shape can be seen [2]. This term makes no assumptions about the object other than it must be of reasonable size and shape relative to its distance from the observer. Hence, the visual range,  $V$ , is

$$V = \frac{1}{\sigma_0} \log_{\epsilon} \left| \frac{C_0}{\epsilon} \right| \quad (3.1)$$

where  $\sigma_0$  is the extinction coefficient,  $C_0$  is the object's *inherent* contrast (no attenuation) with the sky as the background, and  $\epsilon$  is the observer's minimum contrast detection threshold. As is evident in Equation 3.1, the visual range is simply the visibility expressed by an equation.

The meteorological range is defined as the range at which an observer, with a minimum detection threshold of 0.02, can detect a reasonably sized black object. For a black object,  $C_0 = -1$  and  $\epsilon = 0.02$ , Equation 3.1 becomes an estimate of the meteorological range, denoted  $V_1$ ,

$$V_1 = \frac{1}{\sigma_0} \log_{\epsilon} \left| \frac{-1}{0.02} \right| = \frac{3.912}{\sigma_0} \quad (3.2)$$

Estimates of the visibility and visual range are somewhat ambiguous due to variations of different observer's minimum detection thresholds. The minimum detection threshold is the minimum contrast required for an observer to detect an observed target. For example, an observer with a minimum detection threshold of 0.02 will conclude that the visibility is greater than an observer with a threshold of 0.05. Due to this variability in detection thresholds, two observers can estimate different visual ranges under the same meteorological conditions.

Laboratory and field experiments have been conducted to determine the typical minimum detection threshold for the average human. The measured value tends to fall within the range of 0.02 to 0.05. In most modern visibility sensors, a conservative value of  $\epsilon = 0.05$  is used as it correlates well with visibility values reported in

meteorological observations [8, 36, 17]. The visual range becomes

$$V = \frac{3.00}{\sigma_0} \quad (3.3)$$

One of the key factors determining an observer's ability to detect an object under various meteorological conditions is that object's contrast. The observed contrast of a target is defined as the incremental difference in luminance between a target and it's background [7]. In essence, the contrast of an object can vary from -1 to some very large value, as would occur when observing a bright light during a black night. During daytime viewing conditions, the contrast of an object will very rarely exceed a value of 10 [2]. The trivial case occurs when an object and its background emit or reflect the same radiance, resulting in a zero contrast. The mathematical expression for an object's *inherent* contrast, contrast as seen through a vacuum, is given as

$$C_0 = \left| \frac{L_o - L_b}{L_b} \right| \quad (3.4)$$

where  $L_o$  is the object's luminance and  $L_b$  is the background's luminance. When viewing this object through an attenuating medium, such as air, the object's *apparent* contrast is a function of both the range and the extinction coefficient of the optical path. The *apparent* contrast,  $C_a$ , is defined by

$$C_a = C_0 e^{-\sigma_0 R} \quad (3.5)$$

where  $R$  is the distance between the observer and the object. It is understood that this relationship applies when the extinction coefficient is constant across the entire optical path.

A term frequently used to characterize the attenuating characteristics of a medium is known as the optical depth. It represents the scattering and absorbing effects of

molecules, water droplets, particles, etc., present in the atmosphere. The optical depth is the exponent term in Equation 3.5 and is provided below.

$$OD = -\sigma_o R \quad (3.6)$$

This concludes the discussion of human visibility and associated terminology necessary for understanding the visibility sensor design presented in the following sections. The next section discusses the theory of the camera-target setup used to estimate the visibility.

## 3.2 Camera Estimated Visibility

One objective of this research is to evaluate the performance of various enhanced vision systems as they image several active targets under different fog conditions. The need to quantitatively assess the visibility of each fog event, independent of typical human observer variations, is important as it forms a baseline measure required for enhanced vision performance evaluation. The camera-based visibility measurement system is a low cost solution that provides an estimate of the average optical depth, and hence visibility, of the test range. The following discussion substantiates the validity of this system.

### 3.2.1 Estimation Theory

In the context of this thesis, the visibility is estimated by measuring the contrast between a target and its background in a digital image. These *apparent* contrast measurements are related to the extinction coefficient, and hence visibility, in a fashion similar to the presentation in Section 3.1. This section supports the argument that visibility can be estimated via digital images of a specifically designed black and white

target.

As presented in equations 3.4 and 3.5, the *apparent* contrast is related to the *inherent* contrast via the atmospheric attenuation, and both are, in turn, related to the optical depth and visibility. It is evident that if the *apparent* and *inherent* contrasts, along with the distance between observer and target, are known, one could calculate the extinction coefficient, and hence the visibility.

In order to justify using an electronic imaging system in place of a human observer, a brief discussion of perceived contrast is required. The material which follows is based on the theoretical developments found in many texts [55, 56]. The human eye can adapt to an enormous range of light intensity levels illustrated in Figure 3.1. During daytime viewing conditions, photopic vision alone has a range of  $10^6$  millilambert. The visual system does not operate over this entire range simultaneously, rather, the eye adapts to a specific scene brightness, the *brightness adaptation level* or  $B_a$  in Figure 3.1, and has a dynamic range of approximately 2.2 log units about this point. Gonzales and Wintz indicate that this range is comparable with the range achieved by electronic imaging systems [20]. A second major difference between an eye and a camera is the different sensitivity to wavelength. Figures 3.2 and 3.3 illustrate the typical wavelength sensitivity differences between an eye and a CCD camera. The human eye is sensitive up to approximately 700 nm with its peak sensitivity around 550 nm. The CCD camera, on the other hand, is sensitive up to 1000 nm with its peak sensitivity around 500 nm. For the purposes of this visibility sensor, these differences are negligible as the imaged target is a constant black and white. Any substantial deviations between the eye and a typical camera are reduced via calibration discussed later in this chapter. An additional point in support of replacing an observer by an imaging system is the fact that these systems have been designed to mimic human vision as closely as possible. These arguments suggest that the use of a digital camera in place of a human observer is acceptable.

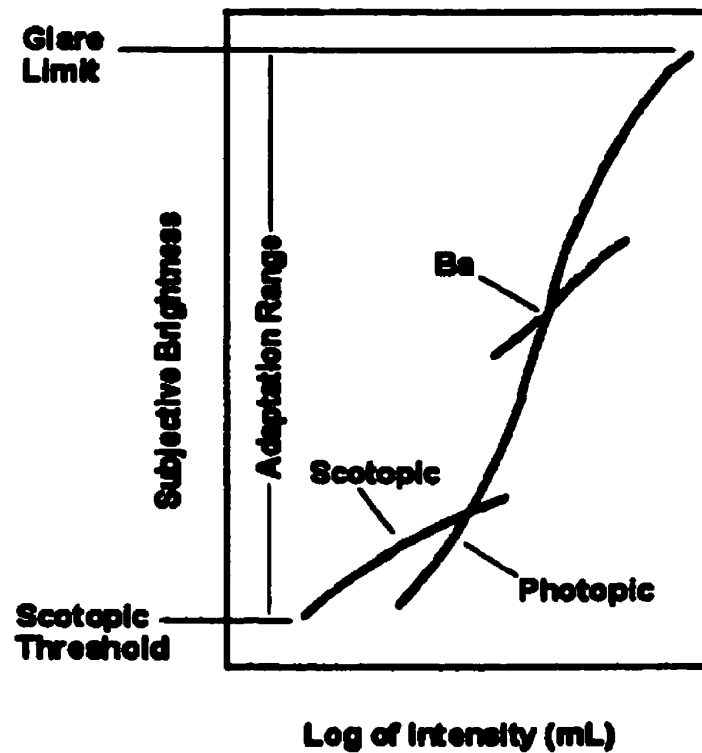


Figure 3.1: Brightness Adaptation (Modified from [20])

The contrast equations developed in Section 3.1 cannot be directly applied for use in this visibility estimation system. These equations are dependent on the perceived contrast of an observer, not the pixel intensity of an image. It is necessary to develop a similar set of equations that account for atmospheric attenuation but depend on the intensity contrast in images. The *apparent* contrast of a digital image,  $C'_a$ , is defined as

$$C'_a = \left| \frac{\gamma_o - \gamma_b}{\gamma_b} \right| \quad (3.7)$$

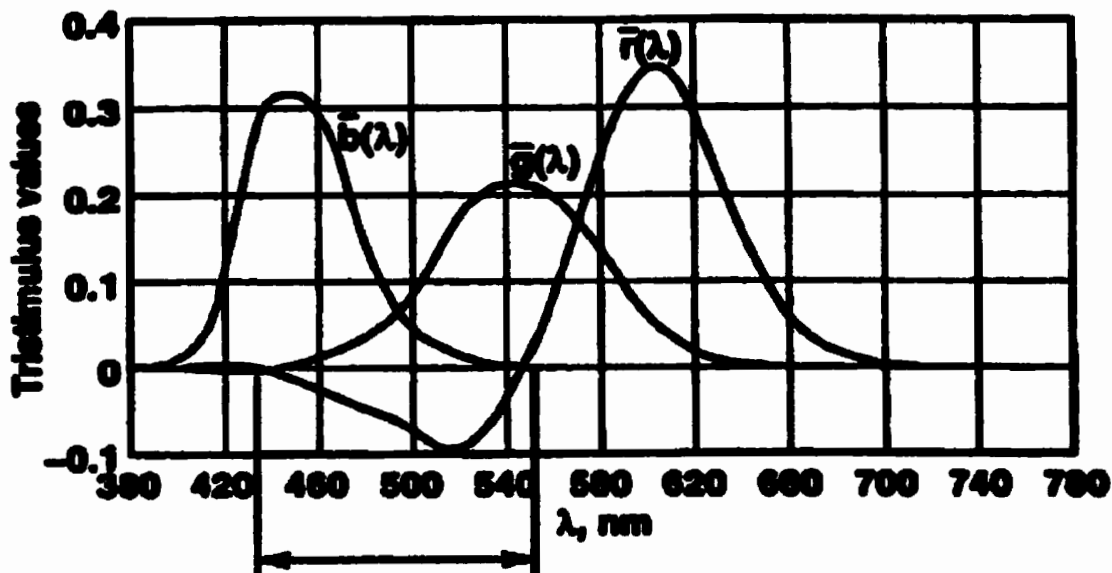


Figure 3.2: Luminosity (Modified from [19])

where  $\gamma_o$  is the object's pixel intensity and  $\gamma_b$  is the background's pixel intensity.

The *inherent* contrast of the target in a digital image can be calculated based on Equation 3.5 by substituting  $C'_s$  for  $C_s$ . The equation for the *inherent* contrast,  $C'_o$ , in a digital image is

$$C'_o = C'_s e^{\sigma_o R} \quad (3.8)$$

Equation 3.8 is the fundamental equation for estimating the visibility using any camera. The *apparent* contrast and the camera-target distance,  $R$ , are known quantities that can be calculated. The next section provides a detailed description of the test setup, the calculation of  $C'_o$ , and the calibration of the visibility estimation system.

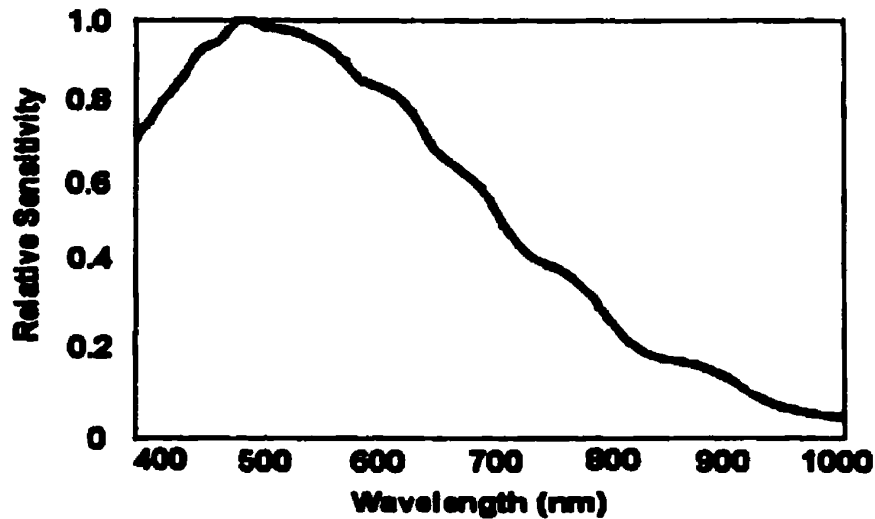


Figure 3.3: Typical CCD sensitivity (Modified from [19])

### 3.2.2 Sensor Calibration

Visibility, as defined in Section 3.1, is based on an observer's ability to detect a black object of reasonable size against the horizon. The visibility estimation system developed in this research project relies on the concepts of visibility theory, but uses a digital camera as opposed to a human observer. This section describes the test setup used to quantify different atmospheric conditions during the calibration trials.

A digital video camera is used to capture images of a painted black and white target under various atmospheric conditions. In addition, targets representing the three primary colors, red, green and blue, have been placed alongside the larger black and white target. The colored targets assisted an investigation into the attenuation of fog on different wavelengths of light. The colored targets, shown in Figure 3.4, are

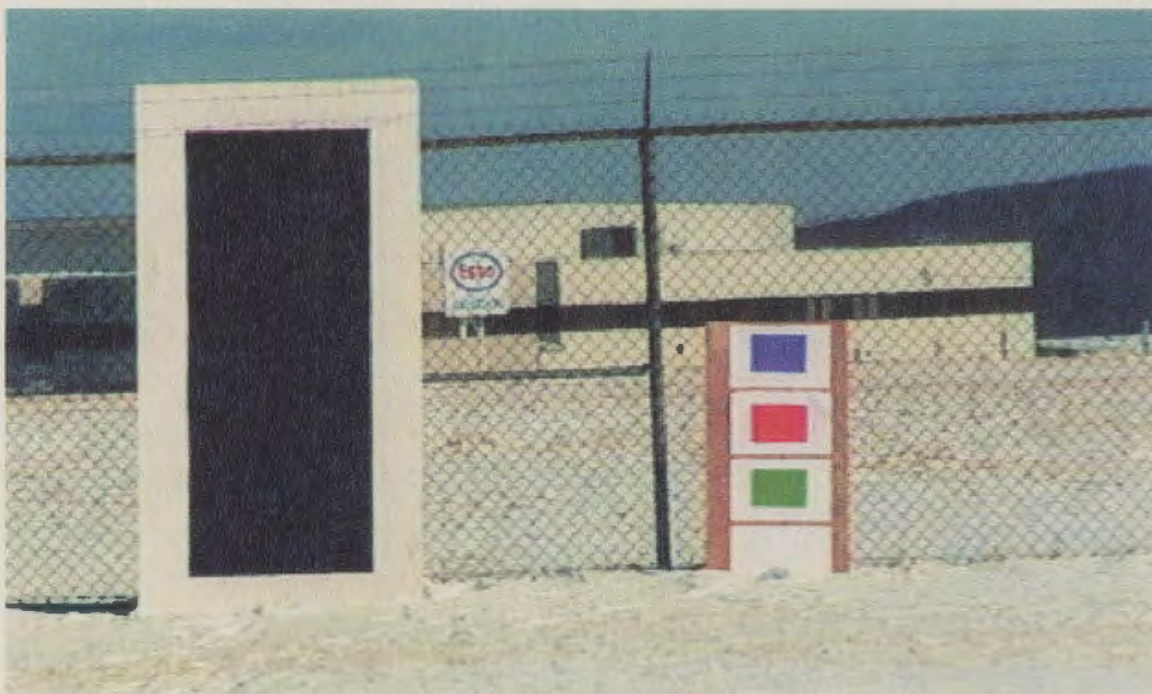


Figure 3.4: Visibility estimation target

not used in the visibility estimation process.

The black and white target is painted on a piece of 4'x8' plywood. The white border, used as the background in the experiments, is approximately 9" wide. The target is located on the ground oriented as shown in Figure 3.4.

Images of the target are captured at ranges of 66m and 102m under both clear and foggy conditions. This determines the impact of range on the target's contrast and the validity of the of the equations developed in Section 3.2.1. Ideally, there should be no noticeable differences in the visibilities estimated from the two different ranges under similar meteorological conditions.

The St. John's International Airport was selected as the calibration site due to the proximity of commercial visibility sensors. Two forward scatter visibility sensors, the

Belfort 6210 and 6220 (referred to as B1 and B3 respectively), record the extinction coefficient at one minute intervals. The sensors are located between the two active runways in the middle of the airfield at a height of 13 feet. B1 and B3 are separated by 100 feet. The camera-target system is located at the edge of the airport's restricted area, approximately 2km from the sensors. The distance between the sensors and camera setup does introduce error, due to the inhomogeneous nature of fog, but this was unavoidable. The extinction coefficient data was provided by Environment Canada.

The extinction coefficient data permits the calculation of  $C'_0$ , the inherent contrast of the black and white target.  $C'_0$  is measured from the image,  $R$  is either 66m or 102m depending on the camera-target distance, and  $\sigma_o$  is measured by the visibility sensors.

The calculation of  $C'_0$  was based on measurements taken 11:43-11:52 am February 23, 2000 under very clear conditions. A plot of the visibility vs. time for February 23 is provided for reference in Figure 3.5. In this figure, there is a significant discrepancy in the visibility readings between sensors B1 and B3. Sensor B3 has recorded the maximum visibility of 60km whereas sensor B1 estimated the visibility between 30-40km. This discrepancy is due to the low level of the forward scattered optical signals (very high visibility) and slight calibration errors inherent in the visibility sensors. The visibility values converge quite nicely for lower visibility conditions. The convergence of the two visibility sensors for low visibility conditions is illustrated in Figure 3.6. The impact of the difference between the two visibility sensors on the calculation of  $C'_0$  is negligible as illustrated in Table 3.1.

Computing the average value for  $C'_0$  from Table 3.1 produces Equation 3.9.

$$C'_0 = 0.8036 \quad (3.9)$$

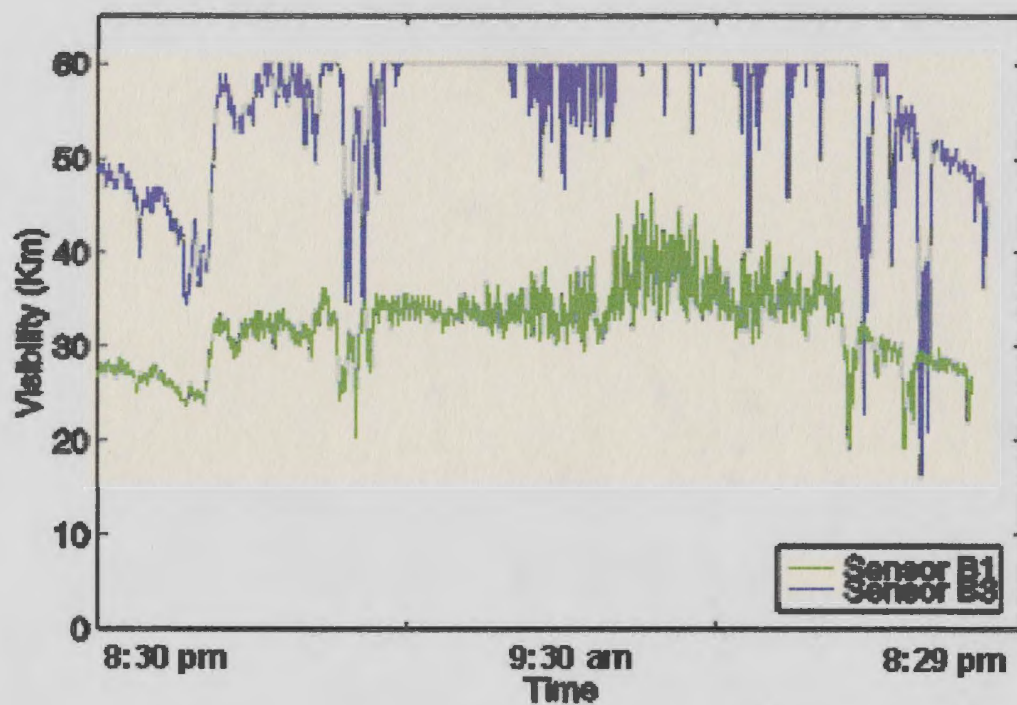


Figure 3.5: Visibility: Belfort visibility sensors, February 23,2000

Table 3.1: Calculation of  $C'_o$

Sensor	R (km)	$\sigma_o$ ( $km^{-1}$ )	$e^{\sigma_o R}$	$\gamma_o$	$\gamma_b$	$C'_a$	$C'_o$
B1	0.066	0.0817	1.0054	40.82	204.93	0.8008	0.8051
B1	0.102	0.0751	1.0077	42.81	211.61	0.7977	0.8038
B3	0.066	0.0500	1.0033	40.82	204.93	0.8008	0.8034
B3	0.102	0.0521	1.0053	42.81	211.61	0.7977	0.8020

Equation 3.9 completes the calibration of the visibility estimation system. The calibration process described above incorporates data from commercial visibility sen-

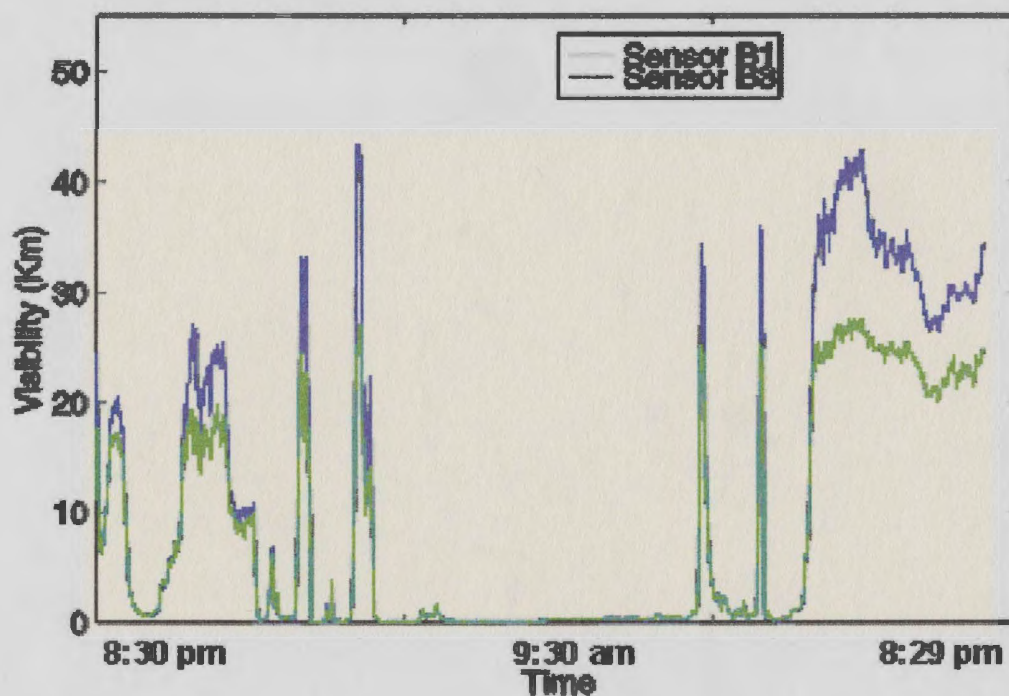


Figure 3.6: Visibility: Belfort visibility sensors, January 12,2000

sors and accounts for errors associated with different cameras and between the camera and human vision.

The next section describes the algorithm designed to extract the targets from foggy images and to measure the intensities of the various regions of interest.

### 3.3 Algorithm

The visibility algorithm presented in this section is designed to extract and measure specified regions of interest (ROI) from a sequence of digital images. Grayscale images are grabbed from a digital video camera and processed using the visibility algorithm. The grabbed image is loaded into memory and the user is prompted to specify the

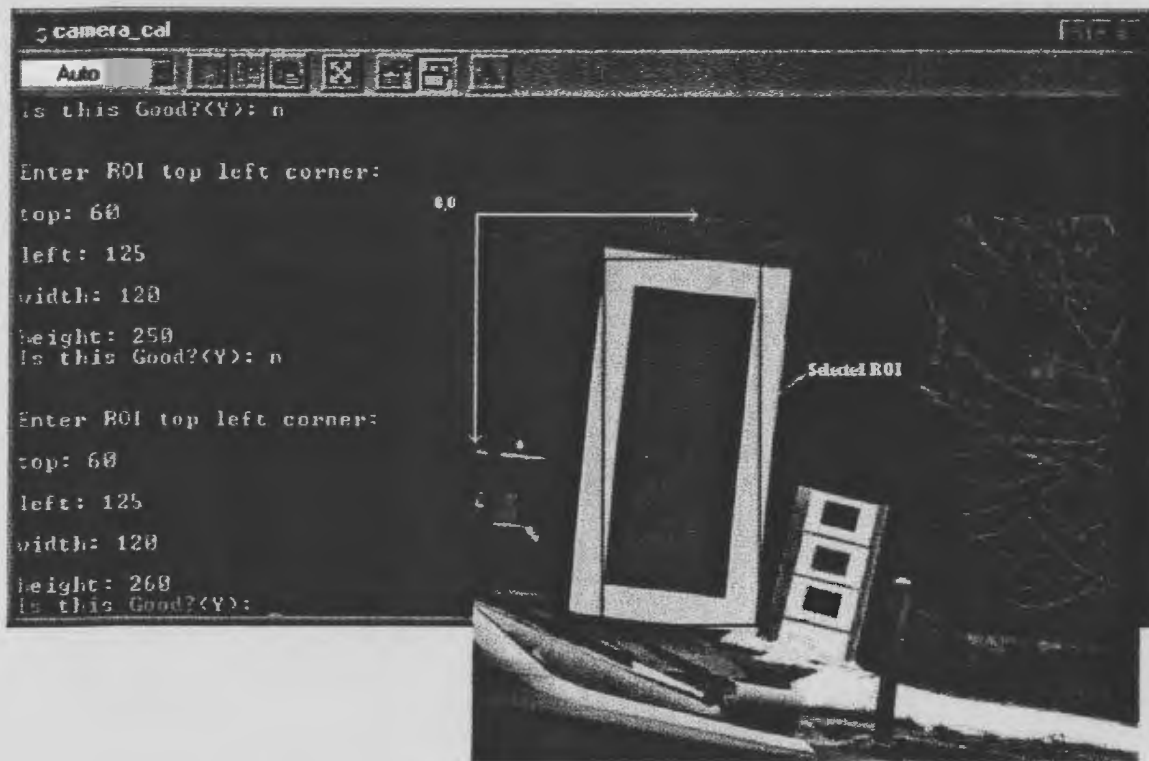


Figure 3.7: Visibility estimation software interface

location, width, and height of the ROI within the image. The user can refine the location and dimensions of the ROI until it is deemed acceptable. The algorithm assumes that the ROI remains fixed throughout the current visibility trial. Should the camera or target move, the ROI must be respecified. The user interface and region selection process is illustrated in Figure 3.7.

Once the ROI has been determined, the region is extracted from the image and algorithm begins in earnest. The visibility algorithm is specified in Figure 3.8 is based on the theory developed in this chapter. The algorithm for computing the visibility from the ROI is written in C++ using the Matrox Imaging Libraries.

A typical histogram of the ROI, similar to the region indicated in Figure 3.7, is

### Visibility Estimation Algorithm

```
Do{
    GrabImage();
    SpecifyROI()
}
While(ROI is not Acceptable? (Y/N));

While(!KeyPress){
    GrabImage();
    ExtractROI();
    ComputeHistogram();
    CalculateApparentContrast();
    ComputeVisibility();
    OutputData();
    Wait10Sec();
}
```

**Figure 3.8: Visibility estimation algorithm**

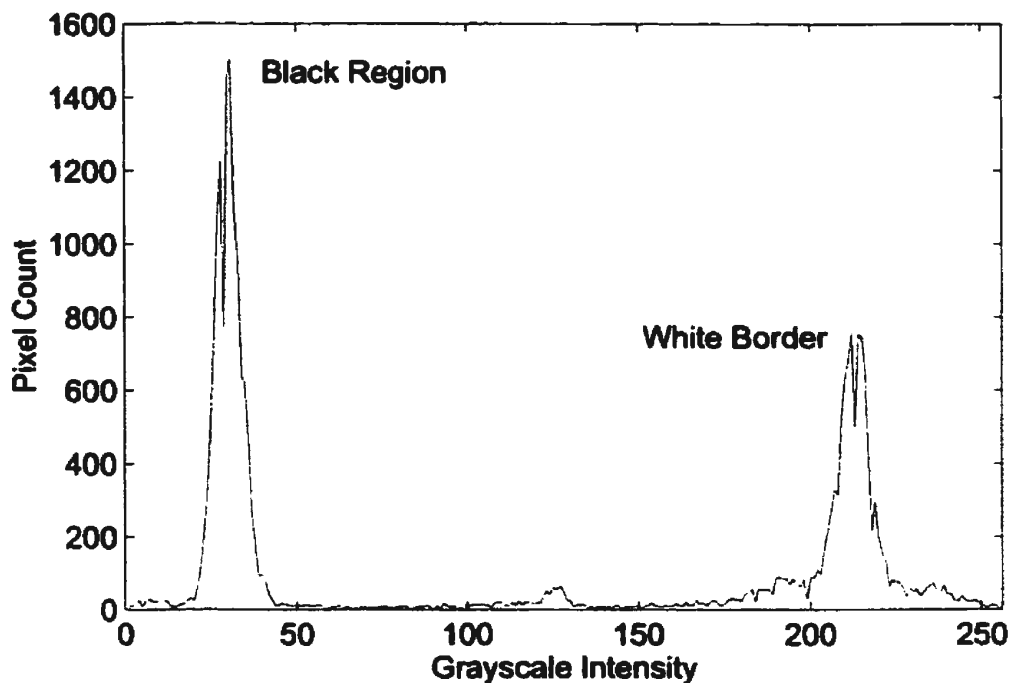


Figure 3.9: Target histogram in clear conditions

presented in Figure 3.9. The histograms typically have two major peaks with the lower peak representing the dark region and the upper peak representing the white background surrounding the dark region. The *apparent* contrast is related to the difference between the two peaks. As the visibility decreases, the distance between the two peaks decreases exponentially as governed by Equations 3.2 and 3.8.

The next section describes the results of the visibility estimation system in comparison with the commercial visibility sensors used at St. John's airport.

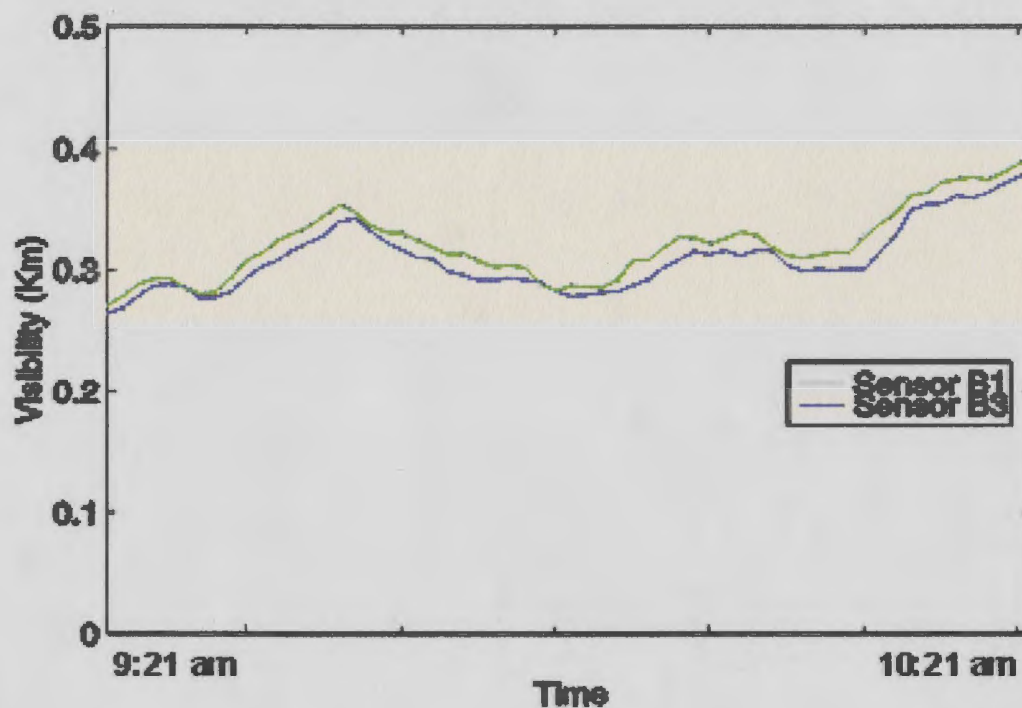


Figure 3.10: Visibility: Belfort sensors, 9:21am-10:21am January 12, 2000

### 3.4 Results

Visibility data was gathered from two commercial visibility sensors, located at the St. John's International Airport, over a two month period. Plots of the visibility data, recorded on January 12, 2000, are presented in Figures 3.10 and 3.11.

During these one-hour periods, images of the black and white target were captured in an open area approximately 2 km from the visibility sensors. The images were processed using the algorithm described in Section 3.3. The visibility estimated via this algorithm is illustrated in figures 3.12, 3.13, and 3.14. Figure 3.12 uses the definition of the visual range to calculate the visibility whereas figures 3.13 and 3.14 use the definition of the meteorological range to provide estimates of the visibility

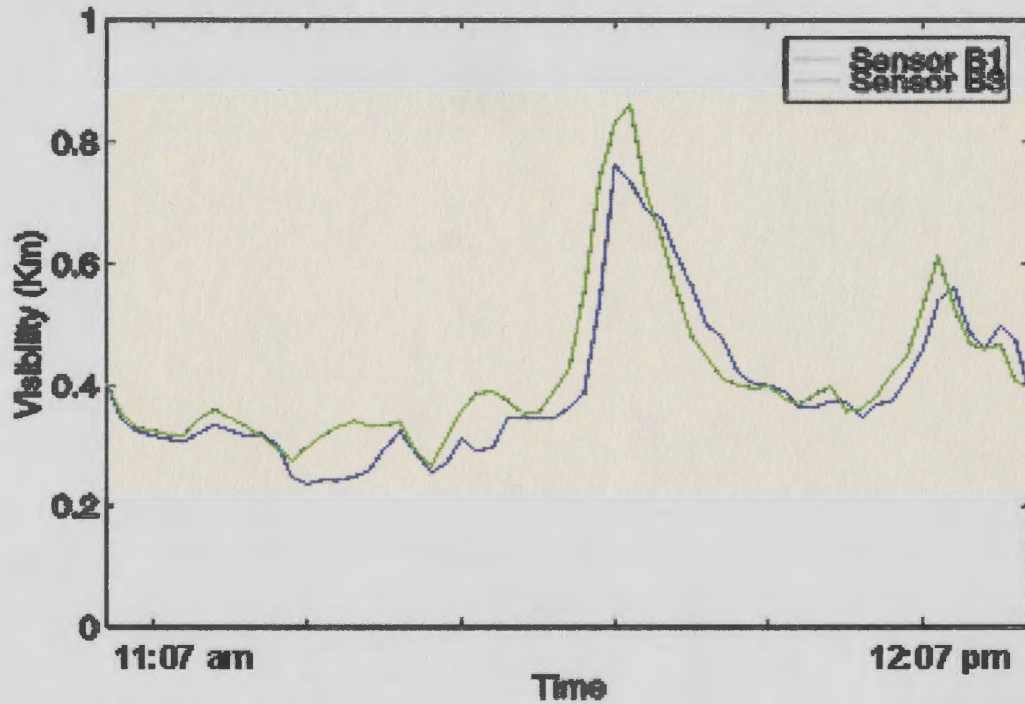


Figure 3.11: Visibility: Belfort sensors, 11:07am-12:07pm January 12, 2000

(See equations 3.2 and 3.3 for details). Comparisons between the commercial sensor readings and these figures indicate that the meteorological range provides the best agreement between the two estimation systems.

As stated in section 3.1, commercial visibility sensors use the visual range, not the meteorological range, to estimate the visibility. Human estimates of the visibility, on the other hand, tend to correlate best with calculations based on the meteorological range. The camera system produces visibility measurements, in-line with commercial sensors, when using the definition of the meteorological range. This makes intuitive sense due to similarities between modern cameras and the human vision system.

Two small gaps are present in the estimated visibility data depicted in Figure 3.13.

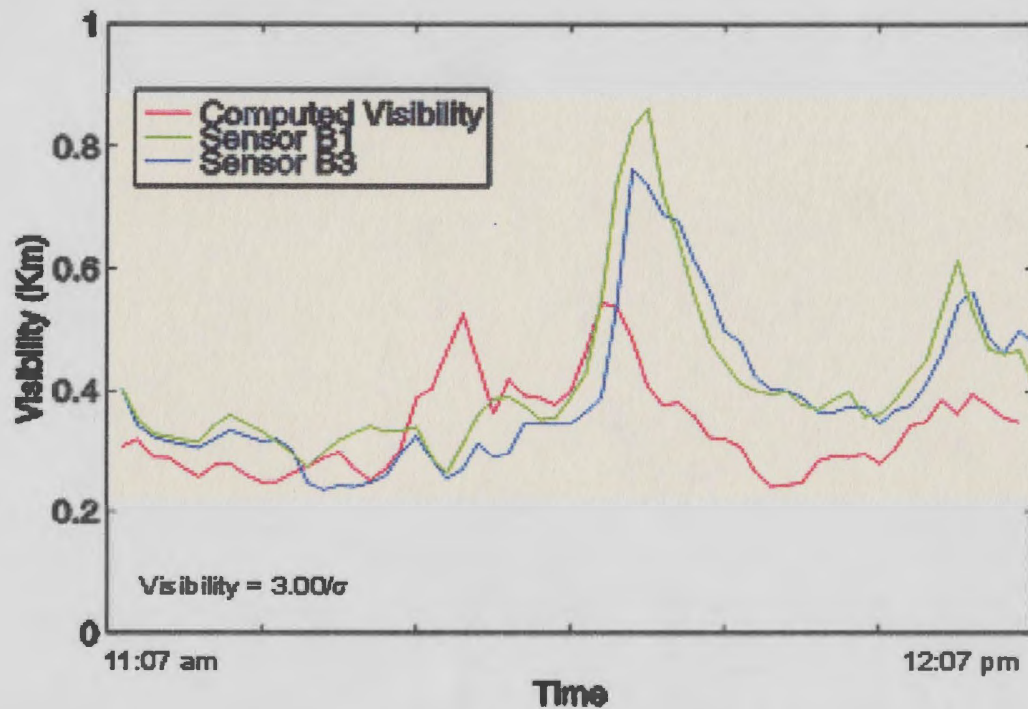


Figure 3.12: Visibility: Image Processing Algorithm using Equation 3.3.

These gaps are due to a visibility less than the distance between the camera and target, and to water buildup on the lens. When the estimated visibility is comparable to the camera-target separation, the target's contrast is reduced to zero and the visibility is recorded as less than this distance.

Examination of the figures presented in the previous paragraphs reveal that there are small differences between the commercial visibility readings and the estimated visibility. These differences are attributed to various sources of error. One source of error was due to the 2 km distance between the camera and the commercial visibility sensors. Spatial and temporal variations in the fog, which is an inhomogeneous medium, produced small variations between the two sets of measurements. A second

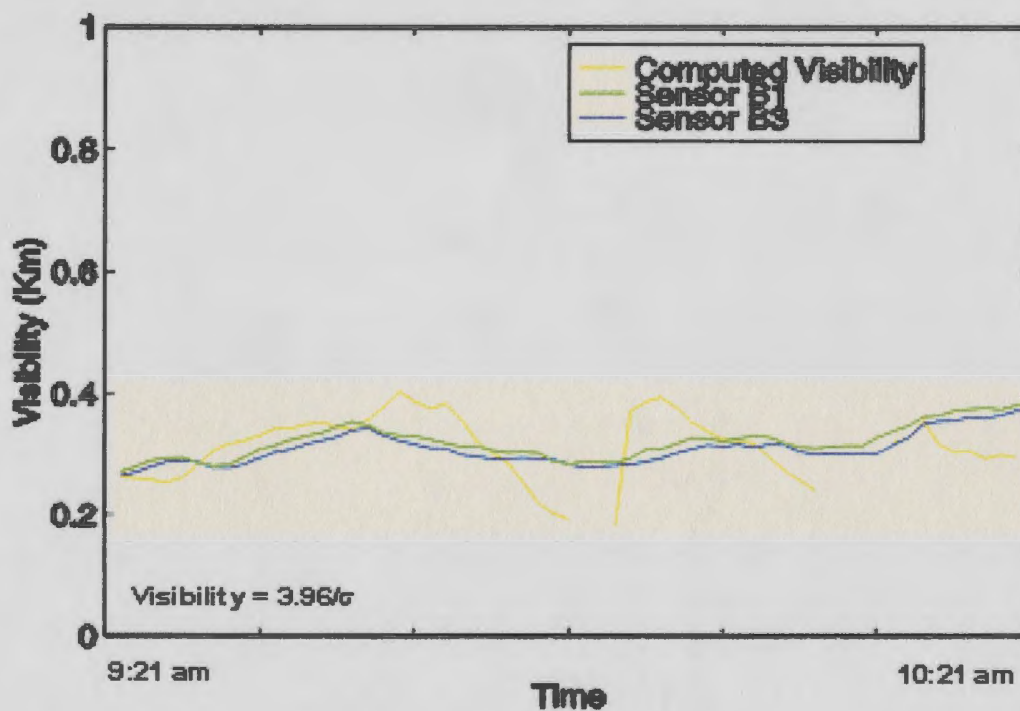


Figure 3.13: Visibility: Image Processing Algorithm using Equation 3.2.

source of error was related to moisture buildup on the camera lens. The camera was encased in a waterproof enclosure except for the lens, which remained in contact with the outside environment. Water droplets on the lens increased the blur and lowered the estimated visibility. Nonetheless, changes in visibility were consistent between both systems.

The theoretical and experimental evidence provided in this chapter support the applicability of this camera-target system as a visibility estimation system. Testing has been conducted over various meteorological conditions and over various ranges and provide similar results as those in this section.

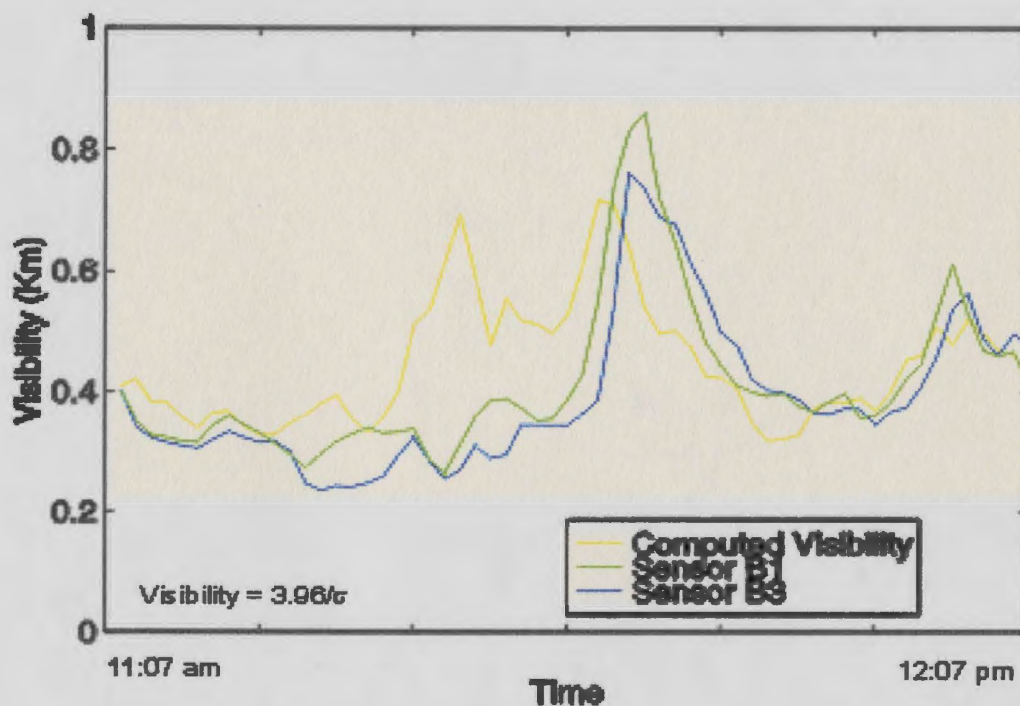


Figure 3.14: Visibility: Image Processing Algorithm using Equation 3.2.

### 3.5 Recommendations

The camera-based visibility system has shown very positive results and is a suitable method for quantifying baseline visibility data. The results agree quite well with commercial visibility sensors and provide a relatively simple, cheap solution capable of autonomous visibility estimation. There are a number of recommendations that will assist further understanding and development of this system.

In comparison to commercial visibility sensors, the camera-based visibility sensor provides a more robust spatial estimate of the visibility than those based on the forward scattering principle. Forward scatter meters have a very short optical paths on which to base their visibility estimates. Spatial and temporal variations

may cause inaccurate readings. The camera visibility system is based on an optical path approximately 100 meters in length, incorporating small spatial variations into the estimate. Commercial visibility meters account for small spatial variations by temporal averaging. Ultimately, this difference is insignificant for most applications.

One problem noted in Section 3.4 was the buildup of moisture on the camera lens. This effect is minimized by placing the camera in a weather shelter preventing water buildup on the camera lens, reducing the blur and increasing visibility estimation accuracy.

This completes the discussion on the design and development of a camera-based visibility estimation system. It has been shown, through experimentation and analysis, that this system provides an accurate estimate of the visibility under various meteorological conditions. This system is employed to collect baseline visibility data for the investigation of enhanced vision performance discussed in the following chapter.

## **Chapter 4**

# **Imaging of Active Targets Through Fog**

**A major obstacle faced by helicopter pilots working offshore Newfoundland is the frequent reduced visibility conditions resulting in lack of situational awareness. In thick fog, the pilots fly based on information obtained from instruments such as radar and GPS. Recently, three high-powered searchlights were mounted on the Hibernia helideck in the attempt to help the pilot obtain a visual reference of the flight deck in foggy conditions. Once the pilot obtains a visual lock on the landing area, he can begin the approach or, if not detected, wave-off and execute a missed-approach. The original motivation for this research sought to understand the potential of various enhanced vision technologies to improve a pilot's ability to obtain visual confirmation of the landing area in fog. While this original motivation remains intact, the applicability of this investigation has expanded to include the automotive, mining, and other harsh environments.**

**This chapter examines the enhanced imaging of active targets using several different imaging modalities. Visible, short-wave IR, mid-wave IR, long-wave IR, and**

polarization difference images of three active targets under various foggy conditions are compared to determine the advantages and disadvantages provided by each system. The key feature used to assess the ability of these systems to image through fog is the contrast between a target and its immediate background. This feature, the fundamental feature of a searchlight or any active target, has been selected to facilitate the comparison of images across several spectral bands. This field study garners experimental evidence indicating the advantages, if any, that various imaging systems might provide to pilots flying to offshore structures in fog.

## **4.1 Experimental Setup**

The active target trials were conducted at Cape Race, a remote location on the southeast coast of Newfoundland that borders on the Grand Banks. This coastal region is characterized by its extremely wet environment, marshy terrain, high winds, and salt air blowing in off the cold Atlantic ocean. The test site was selected based on the frequent occurrence of fog and the similarity to the environment faced by helicopter pilots flying to and from the Hibernia structure.

The experimental setup consisted of a transmit and receive site separated by an optical path approximately 800m long. The background terrain is marshy, containing a significant amount of water and bog, and very little vegetation. The moist terrain provides few thermal details due to the low thermal contrast associated with wet environments. The environment, combined with the high winds, provided a very difficult environment for thermal imaging.

The transmit site was comprised of a power source and three active targets mounted 1m above the ground in an open area exposed to the elements. The receive apparatus was located inside a house containing a window facing the transmit site. The window remained open throughout the duration of the experiment. Various

**Table 4.1: Weather Conditions**

<b>Conditions</b>	<b>Temp(°C)</b>	<b>Rel. Humidity</b>	<b>Wind(km/h)</b>	<b>Visibility(km)</b>
<b>Clear Day</b>	<b>6-10</b>	<b>64%-75%</b>	<b>20</b>	<b>30</b>
<b>Clear Night</b>	<b>1</b>	<b>89%</b>	<b>0</b>	<b>30</b>
<b>Thick Fog: Day</b>	<b>1</b>	<b>95%</b>	<b>30-40</b>	<b>0.150-0.200</b>
<b>Moderate Fog: Day</b>	<b>5</b>	<b>95%</b>	<b>30-40</b>	<b>0.250-0.350</b>
<b>Moderate Fog: Night</b>	<b>1</b>	<b>94%</b>	<b>20-40</b>	<b>0.300-0.400</b>

cameras and computer equipment were placed inside the house to provide protection from the inclement weather. The optical path, between the transmit and receive sites, was approximately 15m above mean sea-level and parallel with the ground.

A number of measurements were recorded at the receive site to assist the characterization of the different fog events. The visibility was estimated using the visibility sensor designed in Chapter 3 and by a human observer using various objects located at different ranges from the receive site. Also, a digital video camera captured visible images representative of the various weather conditions. The temperature, wind speed, and relative humidity were also recorded during the test period. These measurements provided insight into the conditions under which various trials were conducted. The environmental data is presented in Table 4.1

Testing of imaging system performance was conducted over a broad range of weather conditions with emphasis placed on the daytime fog conditions. The images were captured over a series of three days and nights during April 2000.

### 4.1.1 Active Targets

The targets used in this experiment were selected based on availability and practicality of implementation. All three targets were mounted at the transmit site, 1m above ground and 4m from each other.

The targets consisted of a 3000W oven element, two 500W quartz-halogen lamps mounted side-by-side, and a vertically-polarized 150W quartz-halogen searchlight. Under clear dry conditions, the oven element was red hot at full power. The element was modeled as a blackbody radiator at approximately 900K to assist understanding the distribution of output power. The peak emission, around  $2.5\mu\text{m}$ , and spectral distribution of radiated energy from a 900K blackbody are illustrated in Figure 4.1. Under degraded weather conditions, the temperature was lower than 900K due to the cooling effect of the fog and high winds.

Quartz-halogen (QH) sources typically operate at a temperature of around 3300K. The curve for a 3300K blackbody is shown in Figure 4.1. QH sources have their peak emissions around  $1\text{-}2\mu\text{m}$  and radiate substantially more energy in the visible band than a 900K blackbody. This factor is observed by noting the extreme brightness of the QH lamps compared to the dull red glow of the oven element. A significant factor associated with QH sources used in this experiment was that they were contained within an enclosure. The 500W lamps and the 150W searchlight transmitted their energy through a soda-lime glass shield designed to protect the sources from the elements. A typical soda-lime glass lens provides substantial attenuation of wavelengths above  $2.5\mu\text{m}$  as shown in Figure 4.2. The 150W searchlight had an additional polarizing filter mounted over its aperture, further increasing the attenuation of the transmitted radiation. The visible energy radiating from the searchlight was vertically polarized to facilitate the polarization difference imaging experiment. The polarizing film was specified as having 40% transmission across the visible spectrum. The film

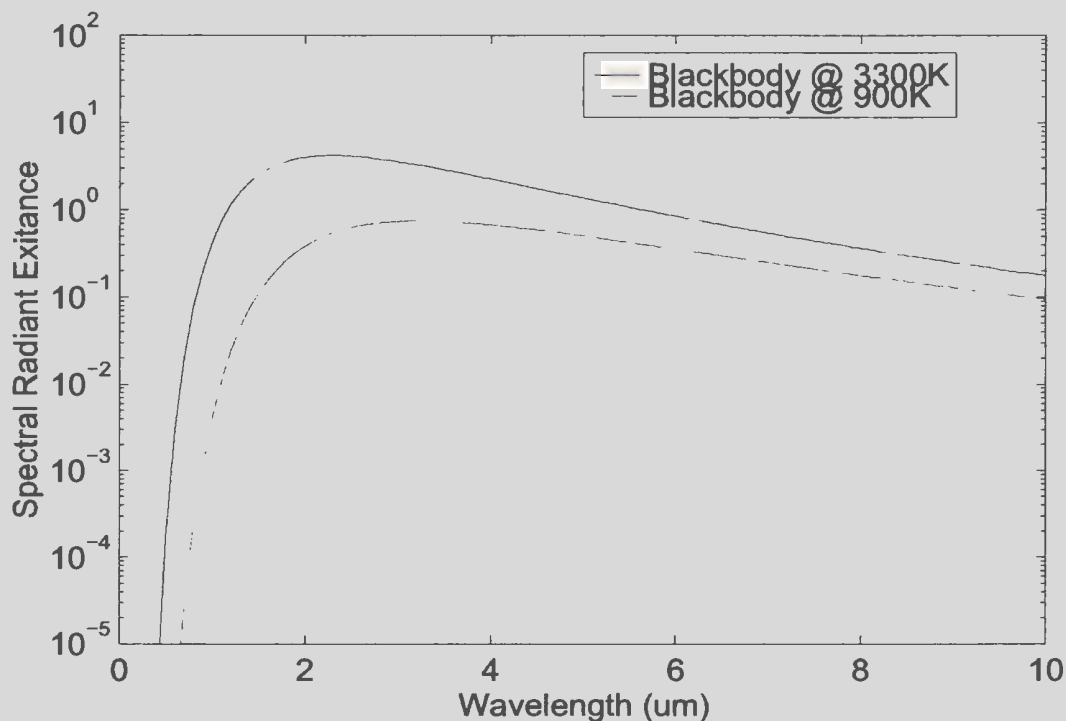


Figure 4.1: Blackbody approximations of a 3000W element and a QH source

was not specified in the infrared region though it is expected to have an attenuating effect. The QH model suggests that these sources will radiate considerable energy in the visible and IR bands below  $2.5\mu\text{m}$ .

An experiment using the infrared imagers, and various lenses, to create a crude spectrometer was conducted to support the theoretical modeling of the active targets. The experiment was performed under clear weather conditions with low humidity, minimizing atmospheric attenuation. The experiment's sole purpose was to support the theoretical modeling of the active targets described in the previous paragraph. Atmospheric attenuation, although significant, was omitted on the basis that it would be present in all imaging circumstances. This omission would not be possible if

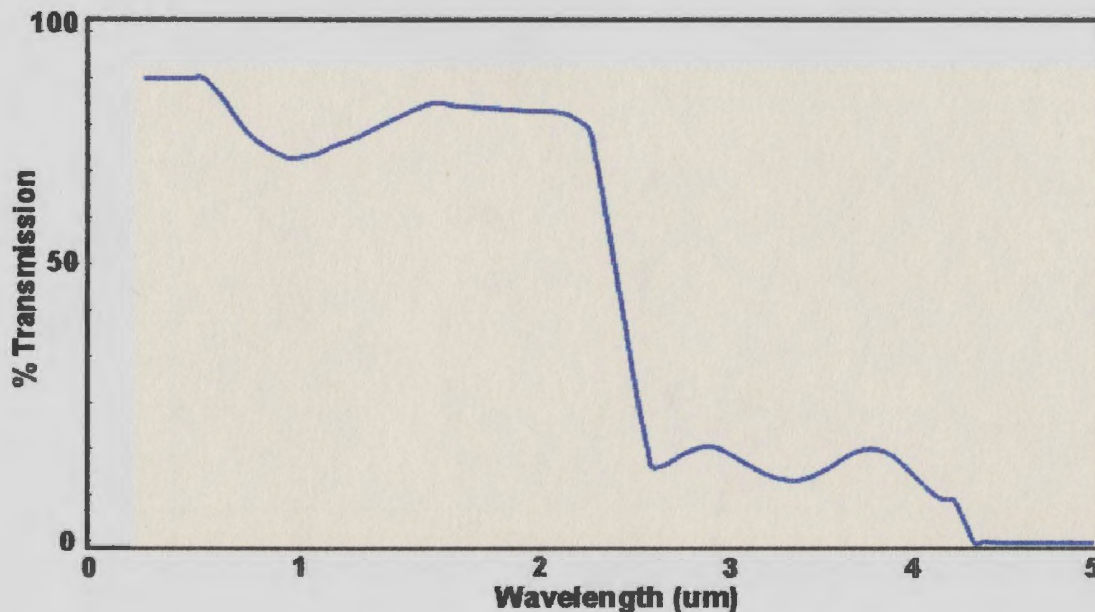


Figure 4.2: Transmission Spectra for Soda-Lime Glass

the goal was to determine the exact transmission characteristics of the targets in a vacuum.

The oven element radiated energy in the 1-2.5 $\mu\text{m}$ , the 3-5 $\mu\text{m}$ , and the 8-12 $\mu\text{m}$  regions as expected. The two 500W QH lamps and the 150W QH searchlight radiated considerable energy in the visible and short-wave infrared (SWIR, 1-2.5 $\mu\text{m}$ ) regions but also significant energy in the 3-5 $\mu\text{m}$  region. The images presented in Figures 4.3, 4.4 and 4.5 illustrate the target's appearance under clear weather conditions in different spectral bands. When imaged in the 4-5 $\mu\text{m}$  region, the element was bright whereas both QH sources were faint but distinct. In the 3-5 $\mu\text{m}$  region, both the IR source and the QH sources were brighter than in the 4-5 $\mu\text{m}$  region, as expected, due to the camera's wider spectral band and soda-lime glass's increased transmissivity.

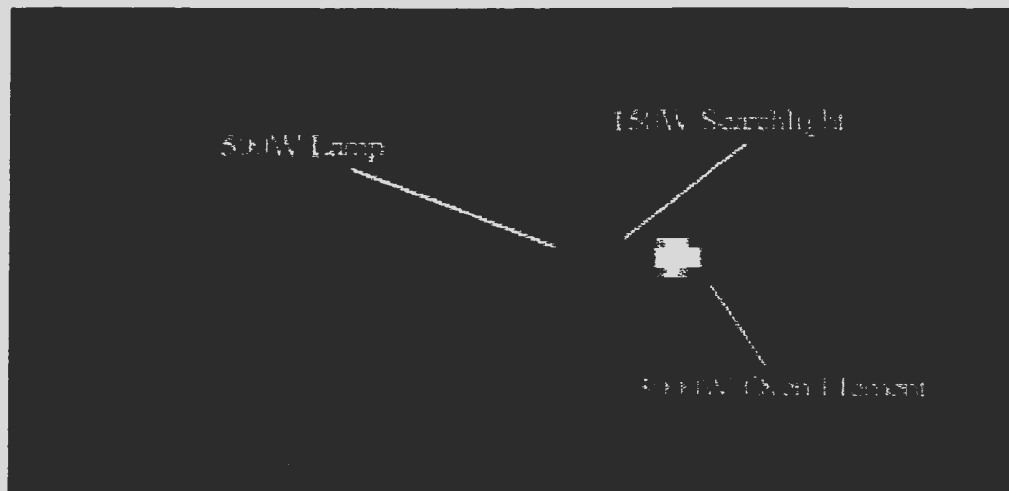


Figure 4.3: Active targets in the  $4\text{-}5\mu\text{m}$  region under clear conditions

Figure 4.5, an image captured in the  $1\text{-}2.5\mu\text{m}$  region, illustrates a large washed-out region surrounding the source, indicating that transmissivity of the soda-lime glass lens has increased dramatically. The increased radiant energy observed in the previous figures support the target models created from blackbody theory and lens attenuation. The oven element radiated energy between  $1\text{-}12\mu\text{m}$  while the 500W lamps and 150W searchlight radiated significant energy below  $4\mu\text{m}$ . These measurements substantiated the target models predictions and provided knowledge of the source's transmission regions.

In addition to the transmission regions, each target directed a different percentage of their total output energy at the receive site. Both the 500W and 150W QH sources had mirrors that focused the radiation towards the imaging systems. The two 500W lamps had a beam divergence of 120 degrees whereas the searchlight had a beam divergence of only 2 degrees. Consequently, the searchlight delivered a much larger percentage of its total energy to the receive site than the 500W lamps. The 3000W

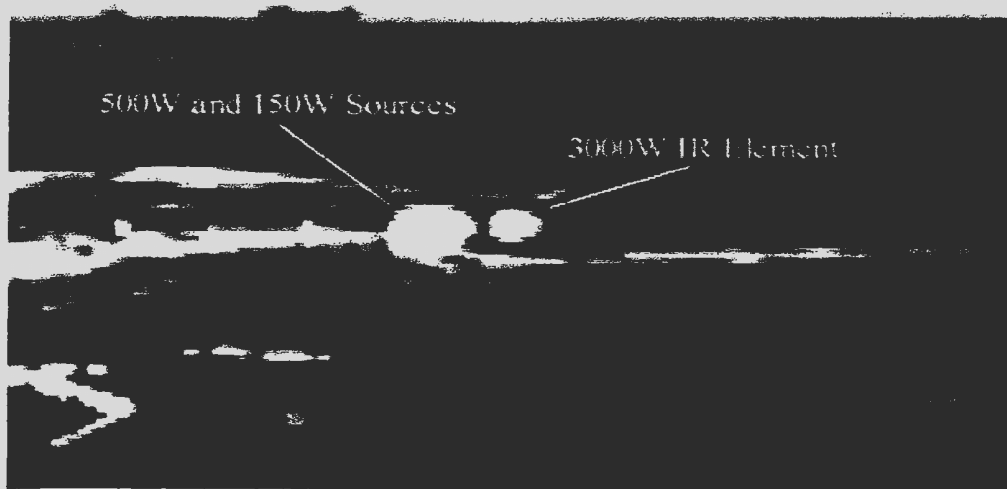


Figure 4.4: Active targets in the 3-5 $\mu$ m region under clear conditions

oven element, having no rear reflector, delivered a much lower power to the observing system than the QH sources.

This discussion provided information regarding the output characteristics of the active sources used in the field experiments. The next section describes the different imaging systems being evaluated and some of their fundamental characteristics.

#### 4.1.2 Enhanced Vision Systems

The field trials discussed in this thesis were designed to evaluate the performance of several imaging systems in marine fog conditions. Visible imaging, polarization difference imaging, and infrared imaging in several bands were examined as these systems were readily available. The infrared regions examined were the 1-2.5 $\mu$ m, 1-5.9 $\mu$ m, 3-5 $\mu$ m 4-5 $\mu$ m, and 8-12 $\mu$ m regions.

Both the visible and polarization difference images (PDI) were captured using a digital video camera. The CCD array is sensitive to energy ranging in wavelength



Figure 4.5: The 500W QH source in the 1-2.5 $\mu$ m region under clear weather conditions

from 350-1000nm with its peak sensitivity around 500nm. The relative sensitivity of a typical CCD camera is illustrated in Figure 3.3 of Chapter 3.

Polarization difference imaging, a second method examined in this work, involved the subtraction of a horizontally polarized image from vertically polarized image. Both the horizontally and vertically polarized images were captured using the visible CCD camera described above. A linear polarizing filter mounted over the lens was rotated through 90° to form these images. This difference image contained information regarding polarization differences found in the scene, notably the vertically polarized searchlight. Figure 4.6 illustrates the concept of polarization difference imaging. The polarization difference image is formed via application of Equation 4.1.

$$pdI(x, y) = I_{\uparrow}(x, y) - I_{\leftrightarrow}(x, y) \quad (4.1)$$

As discussed earlier, the searchlight energy was polarized via a polarizing film mounted directly over the searchlight's aperture. This film attenuated the searchlight energy by approximately 60% in the visible spectrum, resulting in a transmission of

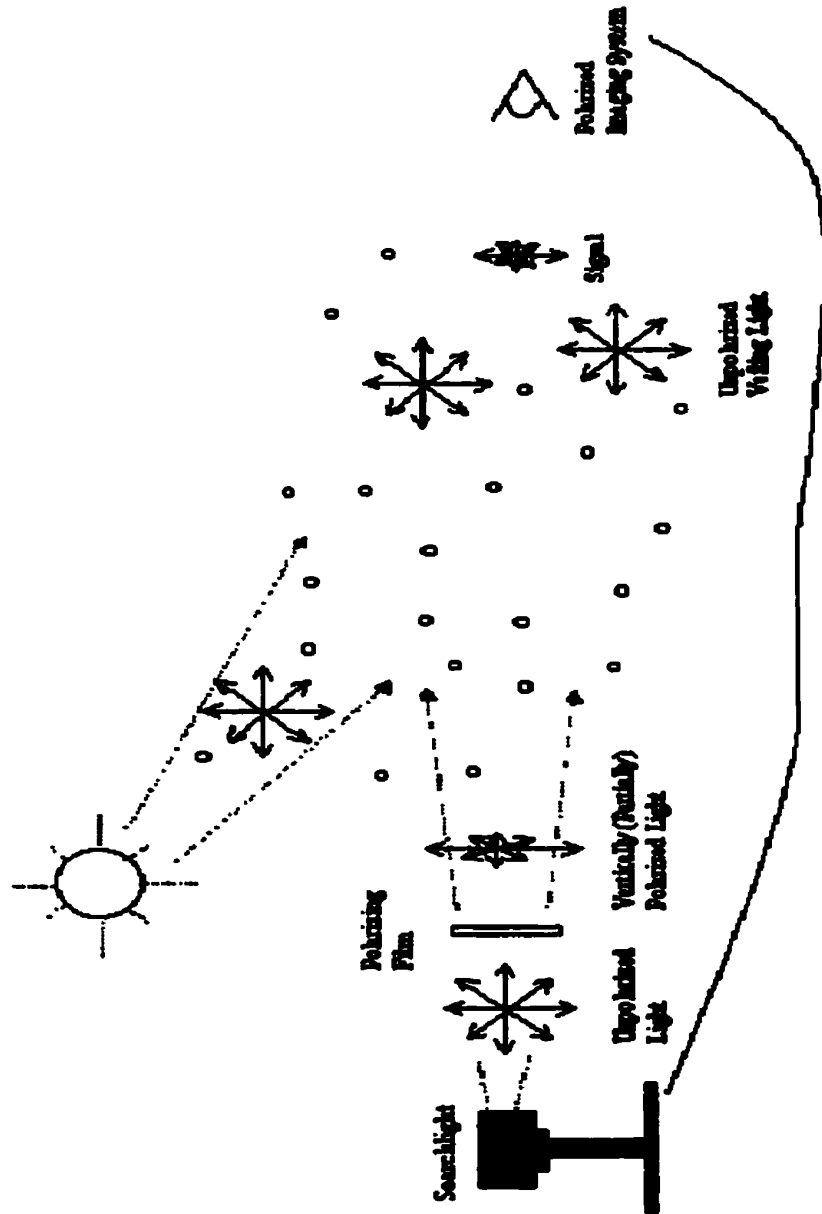


Figure 4.6: The concept of polarization difference imaging

approximately 40%. The film attenuated most of the horizontally polarized energy, which made up about 50% of the total output energy, and approximately 20% of the vertically polarized energy. Another linear polarizing film was mounted over the visible camera's aperture. This filter, when oriented in the vertical direction, attenuated the vertically polarized light from the searchlight by an additional 20% and the unpolarized light from the background scene by 60%. Overall, the signal of interest is attenuated by 20% more than the ambient background scene.

One of the major advantages of polarization difference imaging is its inherent high common mode rejection. The horizontally polarized image provides a sample of the unpolarized signals while the vertically polarized image captures the signal of interest and a sample of the unpolarized signals. Subtraction of the two images provides high common mode rejection and facilitates the use of advanced signal processing techniques. The development and implementation of advanced signal processing algorithms are outside the scope of this thesis.

Two infrared cameras, one in the mid-IR region and one in the long-IR region, were examined during this experiment.

The Mitsubishi IR-U300M1 uncooled camera was used to image the targets in the 8-12 $\mu$ m region under various conditions. The camera had a 320(H)x240(V) silicon detector sensitive and a field of view of  $\pm 18^\circ$  in the horizontal plane.

The relatively wide field of view and low image resolution of the IR-U300M1 presented a significant problem for the experimental setup. Calculations indicated that the camera was capable of imaging a target of 2.3m in width at a range of 800m. The oven element was 0.5m x 0.5m, considerably smaller than the minimum target size. Under clear conditions, the element was imaged as a 4 pixel<sup>2</sup> target but was not visible under any fog conditions. The target was capable of being imaged under clear conditions due to the large temperature contrast between the element and its background. The temperature difference was significantly less under foggy

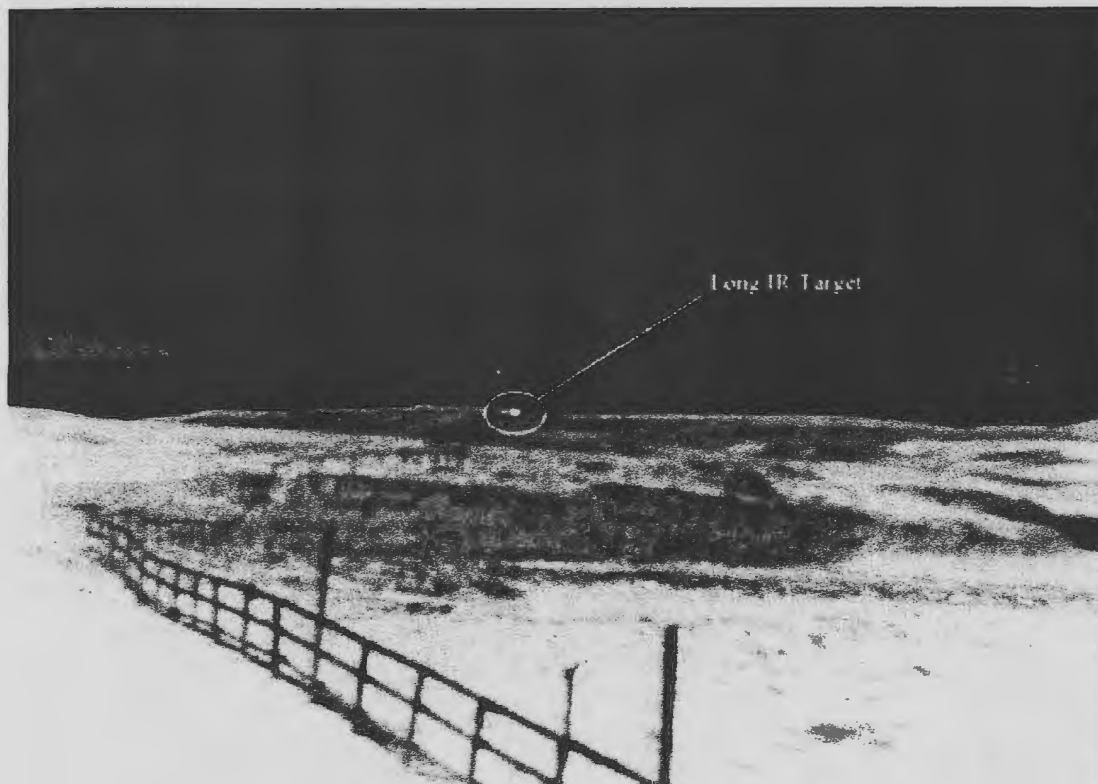


Figure 4.7: Long-IR imaging under clear weather conditions

conditions due to the water's cooling effect on the exposed element. Experimental limitations, such as location of power supplies and extremely rough terrain, prevented the camera-element distance from being reduced. As well, the experiment was designed to examine the effectiveness of the enhanced vision systems to image a target a half nautical mile away. The evaluation of the IR-U300M1 was inconclusive due to the limited spatial resolution and the lens's field of view. Figure 4.7 illustrates the oven element as imaged by the  $8\text{-}12\mu\text{m}$  camera under clear weather conditions.

The Mitsubishi M700 mid-IR camera, in conjunction with several filters and lenses, was used to capture images in four infrared bands in the SWIR and MWIR regions.

The M700 had a platinum silicide detector with an operating temperature of 77K. The camera had a peak sensitivity located at  $2.5\mu\text{m}$  and captured images of scenes in several regions between  $1.2\mu\text{m}$  to  $5.9\mu\text{m}$ . The captured images were  $640\times 480$ , 8-bit grayscale images and were stored on computer for further processing and analysis. The M700 had zoom capabilities permitting up to 8 times magnification. Two internal filters facilitated image capture in the  $1.2\text{-}5.9\mu\text{m}$  and the  $4.0\text{-}5.9\mu\text{m}$  regions. A 50mm Mitsubishi lens, with a horizontal field of view of  $\pm 7^\circ$ , passed  $3\text{-}5\mu\text{m}$  wavelength energy to the imaging system. This lens in combination with the two internal filters allowed image capture in the  $3\text{-}5\mu\text{m}$  and  $4\text{-}5\mu\text{m}$  regions. A 25mm Applied Physics Specialties lens, with a horizontal field of view of  $\pm 20^\circ$ , passed wavelengths between  $1.3\text{-}5.9\mu\text{m}$ . A glass filter was mounted on this lens to image in the  $1.3\text{-}2.5\mu\text{m}$  region. In total, the M700 camera captured images in the  $1.3\text{-}5.9\mu\text{m}$ ,  $1.3\text{-}2.5\mu\text{m}$ ,  $3\text{-}5\mu\text{m}$ , and  $4\text{-}5\mu\text{m}$  spectral bands. These regions correspond to several transmission windows in the atmosphere shown in Figure 4.8.

## 4.2 Imaging Results

Images were captured under daytime and nighttime conditions with the primary interest in the daytime performance. Transport Canada regulations permit daytime helicopter flights to the Hibernia GBS, establishing the need to evaluate the enhanced visions system performance under daytime fog conditions. Experimental data was collected and analyzed under nighttime fog conditions to support the daytime analysis and facilitate overall system characterization.

An absolute comparison between the different imaging systems described above was difficult due to the diversity of the cameras and targets involved. The salient feature for comparison was determined to be the intensity contrast between each target and its background. The intensity contrast provided a common basis for

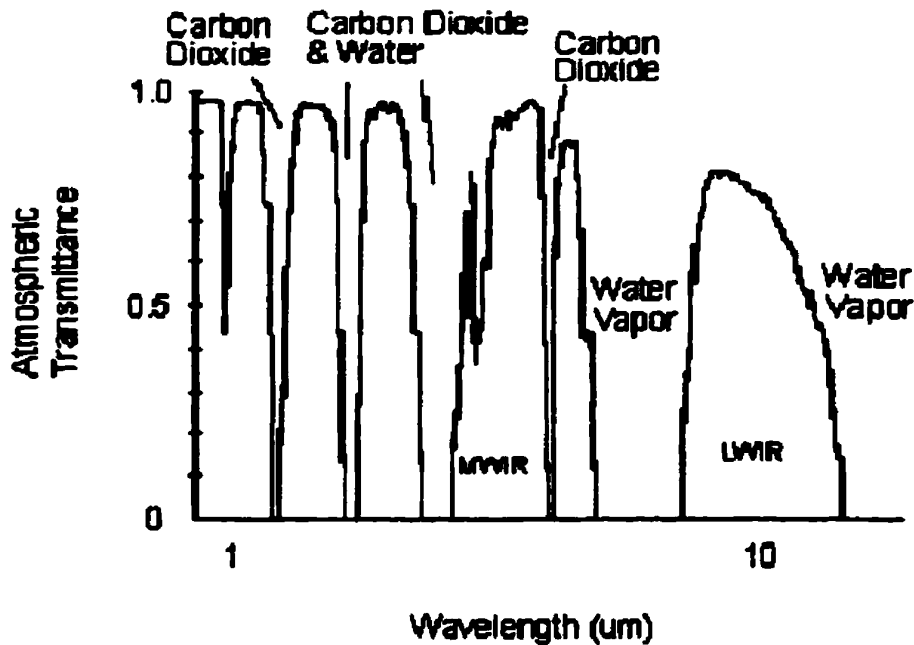


Figure 4.8: Atmospheric transmission windows

comparison as each target was a large source of radiant energy albeit in different spectral regions. Other features, such as size and shape, could not be justified as they were range dependent, see the discussion in Chapter 3, and were distorted by the fog.

The average grayscale intensity of each target was compared to the average intensity of the immediate background and the local contrast calculated using Equation 3.7. The calculated daytime contrasts between target and background for each imaging system are illustrated in Table 4.2 while nighttime contrasts shown in Table 4.3. Several measurements were not captured due to incompatible target-camera characteris-

tics, such as a visible image of the oven element, or due to accidental omissions. These measurements are represented by a '-' in Tables 4.2 and 4.3. The data presented in Tables 4.2 and 4.5 has been normalized by the largest contrast in each column and presented in Tables 4.4 and 4.3 for comparison purposes. The contrast measurements were based on an average of 5 images captured over a 1 minute time interval. The temporal averaging served to reduce sensor noise and weather variations.

Daytime images of the targets were recorded in 150-200m visibility but targets were not visible. A helicopter pilot flying to the Hibernia structure in these conditions would have to execute a missed approach and return to St. John's. The imaging systems examined in this thesis provided no visual enhancements under 150-200m visibility conditions.

In many conditions, particularly clear day and night conditions, the visible imaging system was saturated by the active target. Saturation limited the calculated contrast ratios to a small extent, depicted in Tables 4.2 and 4.3, but not significantly. Examination of Equation 3.7 shows that the dominant term is the local background intensity in the denominator. Clipping of the active target intensities introduced small errors in the contrast calculations but was unavoidable due to lack of attenuating filters.

#### **4.2.1 Visible Imaging**

Visible imaging provided reasonable performance under night and clear day conditions. During the clear day conditions, the contrast was limited by higher intensity of the background, as illustrated in Table 4.6 though the lights were still quite visible. Both the 150W and 500W QH sources caused the visible sensor to saturate under clear night conditions but still resulted in quite good performance as illustrated in Table 4.5.

The contrast ratio ranged 0.1-0.5 during the moderately foggy daytime conditions,

Table 4.2: Day contrast measurements

System	Day -Vis: 30 km			Day -Vis: 0.250-0.350 km		
	150W QH	500W QH	3kW Elem	150W QH	500W QH	3kW Elem
Visible	2.25	1.44	-	0.534	0.102	-
PDI	10.75	-	-	23.7	-	-
IR (1.3-2.5 $\mu$ m)	-	0.951	0.968	(2.19)	(2.19)	1.52
IR (3-5 $\mu$ m)	(5.97)	(5.97)	5.97	(0.114)	(0.114)	0.130
IR (4-5 $\mu$ m)	0	4.57	5.31	0	0	0
IR (1-5.9 $\mu$ m)	-	-	-	(2.38)	(2.38)	2.31

( )  $\rightsquigarrow$  targets have merged due to blooming

-  $\rightsquigarrow$  target not captured

Table 4.3: Night contrast measurements

System	Night -Vis: 30 km			Night -Vis: 0.300-0.400 km		
	150W QH	500W QH	3kW Elem	150W QH	500W QH	3kW Elem
Visible	24	24	-	7	6.36	-
PDI	20.30	-	-	12.5	-	-
IR (1.3-2.5 $\mu$ m)	-	-	-	(1.07)	(1.07)	0
IR (3-5 $\mu$ m)	(2.29)	(2.29)	(2.29)	(8.30)	(8.30)	(8.30)
IR (4-5 $\mu$ m)	0	3.24	3.28	0	0	0
IR (1-5.9 $\mu$ m)	(1.93)	(1.93)	(1.93)	(7.52)	(7.52)	(7.52)

( )  $\rightsquigarrow$  targets have merged due to blooming

-  $\rightsquigarrow$  target not captured

Table 4.4: Normalized day contrast measurements

System	Day -Vis: 30 km			Day -Vis: 0.250-0.350 km		
	150W QH	500W QH	3kW Elem	150W QH	500W QH	3kW Elem
Visible	2.1	2.4	-	0.2	0.4	-
PDI	10.0	-	-	10.0	-	-
IR (1.3-2.5 $\mu$ m)	-	1.6	1.6	0.9	9.2	6.6
IR (3-5 $\mu$ m)	5.6	10.0	10.0	0.1	0.0	0.1
IR (4-5 $\mu$ m)	0.0	7.7	8.9	0.0	0.0	0.0
IR (1-5.9 $\mu$ m)	-	-	-	1.0	10.0	10.0

Table 4.5: Normalized night contrast measurements

System	Night -Vis: 30 km			Night -Vis: 0.300-0.400 km		
	150W QH	500W QH	3kW Elem	150W QH	500W QH	3kW Elem
Visible	10.0	10.0	-	5.6	7.7	-
PDI	8.5	-	-	10.0	-	-
IR (1.3-2.5 $\mu$ m)	-	-	-	0.9	1.3	0.0
IR (3-5 $\mu$ m)	0.1	0.1	7.0	6.6	10.0	10.0
IR (4-5 $\mu$ m)	0.0	0.1	10.0	0.0	0.0	0.0
IR (1-5.9 $\mu$ m)	0.1	0.1	5.9	6.0	9.1	9.1

Table 4.6: Visible target-background intensity measurements

	Background	150W QH	Contrast	500W QH	Contrast
Clear Day	76.1	247.5	2.25	186.0	1.44
Clear Night	10	250	24	250	24
Day: Vis 0.250-0.350 km	158.0	242.4	0.534	174.1	0.102
Night: Vis 0.300-0.400 km	32.0	239.0	7.00	239.0	6.36

quite low when compared to several of the Mid-IR cameras and the PDI system. Overall, the visible camera ranked ahead of the 3-5 $\mu$ m and 4-5 $\mu$ m IR cameras but well behind the PDI, 1-2.5 $\mu$ m and 1-5.9 $\mu$ m imaging systems under the day fog conditions.

Examples of these images under moderate daytime fog and moderate nighttime fog are shown in figures 4.9 and 4.10 respectively.

Successful detection of the active targets under the day fog conditions was noted to be very difficult using the human eye. On several occasions, the active targets were readily identified on video but required significant time to locate in the natural environment. It is hypothesized that a computer vision system capable of target detection and tracking would add significant value to offshore aviation in inclement weather. Such a system would indicate a narrow region of interest, directing a pilot to search this region for the targets. These results indicate that additional research is required to examine the efficiency of visible imaging in comparison to human imaging of active targets in fog.

The chief advantage of the visible camera is its simplicity and mature technological level. A suitable visible imaging system can be purchased for several thousand dollars and integrated into an automatic target acquisition and tracking system with the assistance of additional computing power. A sophisticated algorithm would be

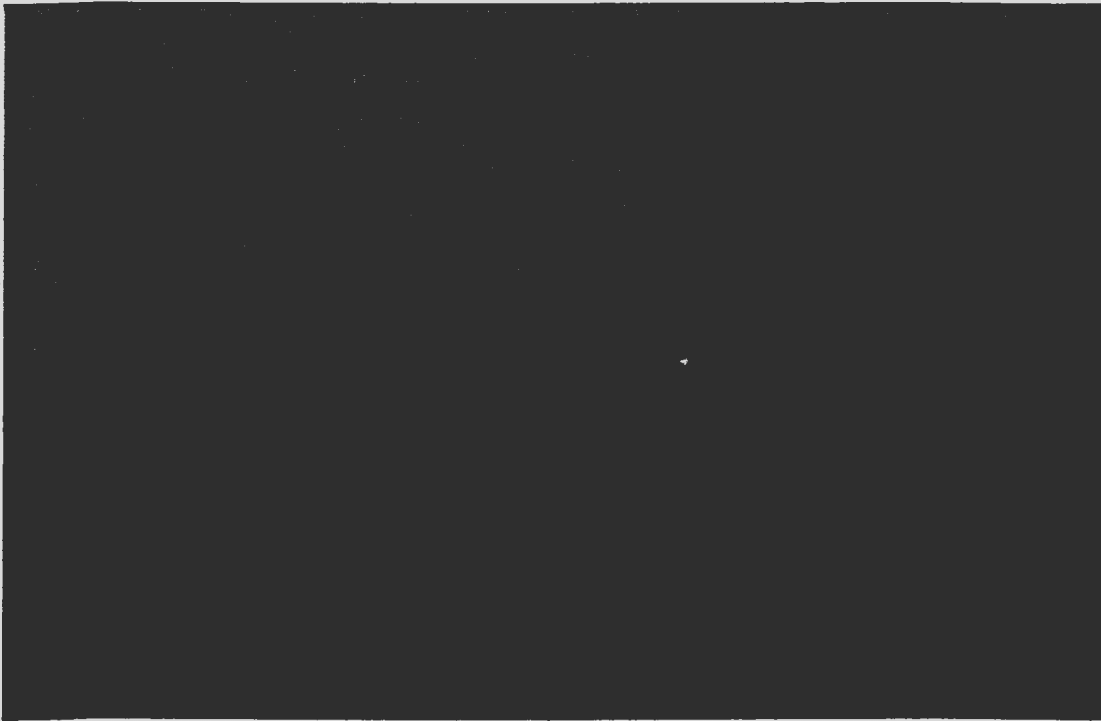


Figure 4.9: Visible image of active targets: Day visibility 0.250-0.350 km

required to autonomously acquire and track the correct target while rejecting other bright targets such as the flare boom or bright patches of fog.

#### 4.2.2 Polarization Difference Imaging

Based on the measure of contrast ratio, polarization difference imaging was the best imaging modality for the purposes of target acquisition and tracking based on the measure of the contrast ratio. In all weather conditions excluding the thick fog conditions (visibility 0.150-0.200km), PDI achieved a contrast higher than 10, much better than the other imaging systems whose contrast ranged between 0.5-3. The PDI system had a contrast ratio of 23.7 during daytime fog conditions whereas the

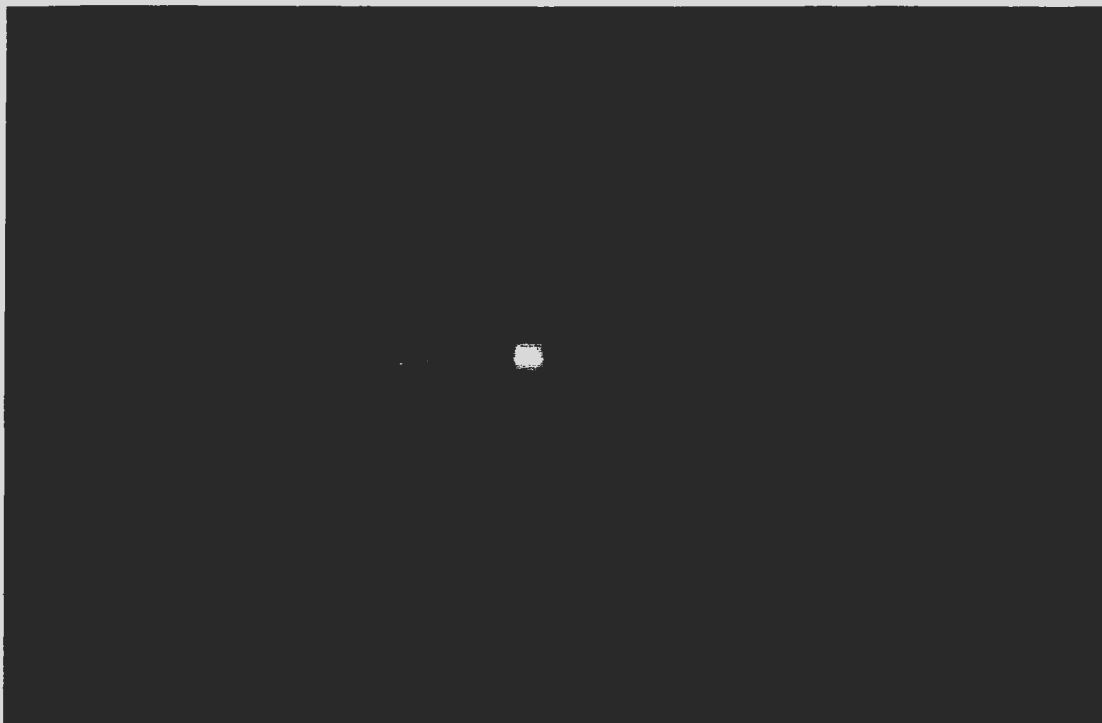


Figure 4.10: Visible image of active targets: Night visibility 0.300-0.400 km

1.0-5.9 $\mu\text{m}$  IR camera only achieved a contrast ratio of 2.38. The measured intensities of the target and background in the PD image are shown in Table 4.7

The high common mode rejection of the polarization difference system provided a high contrast for imaging the active target daytime visibility ranging between 0.250-0.350 km. This resulted in good distinction between the target and its background, providing an excellent base system for target tracking through the fog. The horizontal, vertical, and polarization difference image under moderate daytime fog conditions is shown in figure 4.11

The common mode rejection simplifies the acquisition and tracking algorithm by rejecting common bright areas that might be confused with the target of interest. The

**Table 4.7: PDI target-background intensity measurements**

	<b>Background</b>	<b>150W QH</b>	<b>Contrast</b>
<b>Clear Day</b>	<b>12.4</b>	<b>145.7</b>	<b>10.75</b>
<b>Clear Night</b>	<b>8.7</b>	<b>185.1</b>	<b>20.3</b>
<b>Day: Vis 0.250-0.350 km</b>	<b>3.3</b>	<b>81.5</b>	<b>23.7</b>
<b>Night: Vis 0.300-0.400 km</b>	<b>13.5</b>	<b>181.5</b>	<b>12.5</b>

system detects differences in polarization states causing bright, unpolarized targets to be rejected upon formation of the PD image. Also, fog causes polarized light to lose its polarization state due to its random scattering nature. Weakly polarized targets are prevented from propagating through the fog while strongly polarized co-operative targets would maintain partial vertical polarization, detectable by the imaging system. The PDI system facilitates a target acquisition and tracking algorithm design capable of hardware implementation using simple thresholding techniques. The simplicity of design and implementation enables a low-power, compact system to be constructed and installed in a helicopter where power, weight and space are limited.

It was noted during the experiment that the PDI system did not provide a noticeable increase of the visual detection range of the active target when compared to standard visible imaging. The primary advantage of this system is the high common mode rejection and the inherent target acquisition and tracking characteristics. Ultimately, a PDI-based system could be used to decrease the visual workload and increase the detection efficiency of a pilot trying to detect the approach lights in a fog.

The benefits of a PDI-based system are its ease of implementation, low cost, high common mode rejection, low-power requirements, compact size, and inherent



**Figure 4.11: Horizontal, vertical, and polarization difference images: Daytime visibility 0.250-0.350km**

acquisition and tracking features. A proposed PDI system has been designed and is presented in Chapter 5.

### **4.2.3 Infrared Imaging (1-2.5 $\mu\text{m}$ )**

Images of the targets in the SWIR region, 1-2.5 $\mu\text{m}$ , captured under moderately foggy daytime conditions, had much better contrast ratios than those captured in the visible spectrum. Under these conditions, the SWIR images had contrasts of 2.19 and

1.52 for the lights and element, respectively, compared to the visible images that attained a maximum contrast of 0.534. SWIR camera performance was poor under nighttime fog conditions achieving a contrast of 1.07, well below the performance of the other systems. The target and background intensities used to calculate the SWIR image contrast are given in Table 4.8. The measurements denoted by a '-' represent unintentional omissions.

**Table 4.8: SWIR target-background intensity measurements**

	Background	150W QH	500W QH	3kW Elem
Clear Day	112.9	-	220.3	222.2
Clear Night	-	-	-	-
Day: Vis 0.250-0.350 km	76.1	242.7	242.7	191.5
Night: Vis 0.300-0.400 km	116.5	241.1	241.1	116.5

The performance discrepancy is evident in the SWIR images captured during the day and night conditions. This is attributed to problems associated with lens calibration in the 1-2.5 $\mu$ m and 1-5.9 $\mu$ m regions encountered during the field trials. The Mitsubishi mid-IR camera and Applied Physic's lens combination required manual calibration. A uniform temperature target must be placed in front of the APS lens during calibration, preventing internal reflections and image distortion. Unfortunately, this problem was not discovered until after the cameras had been returned. Additional testing is required to verify these results and confirm IR imaging performance in the SWIR region. The captured images still provided representations of the active targets with some minor distortion. SWIR image captured during nighttime fog conditions with the distortion is shown in Figure 4.12. The calibration problems encountered in the 1-2.5 $\mu$ m and 1-5.9 $\mu$ m regions were not encountered in any other



Figure 4.12: SWIR image of the targets under nighttime fog conditions

spectral region.

Overall, imaging in the SWIR region in moderate daytime fog was better than imaging in the mid-IR region but not quite as good as imaging in the 1-5.9 $\mu\text{m}$  band. It is hypothesized that imaging in the SWIR and 1-5.9 $\mu\text{m}$  regions would increase the range at which the targets could be acquired but only marginally at best. This is evident in the fact that the IR contrast was significantly higher than contrasts measured in the visible regions under 0.250–0.350 km visibility and that none were detected in 0.150–0.200 km visibility. If target detection range was the fundamental consideration, some marginal advantages could be obtained using a matched target-detection system in the SWIR region. In terms of adding value to commercial offshore

aviation operations, this system proved too expensive, totaling \$100k, and provided little benefit over existing systems.

#### 4.2.4 Infrared Imaging (1-5.9 $\mu$ m)

Imaging in the 1-5.9 $\mu$ m infrared region used the same camera and lens setup as used in the SWIR region with the exception of a glass filter. This filter, which blocked radiation above 2.5 $\mu$ m, was removed, making the system sensitive to the entire 1-5.9 $\mu$ m band. This system ranked second overall in performance under daytime fog conditions, achieving a contrast of 2.4, behind that of the PDI system but ahead of the other imaging systems. An image captured in the 1-5.9 $\mu$ m region under 0.250-0.350 km visibility conditions is shown in Figure 4.13 and the intensity measurements depicted in Table 4.9. Measurements represented by a '-' are due to unintentional omissions.

Table 4.9: 1-5.9 $\mu$ m target-background intensity measurements

	Background	150W QH	500W QH	3kW Elem
Clear Day	-	-	-	-
Clear Night	84.0	246.2	246.2	246.2
Day: Vis 0.250-0.350 km	74.1	250.6	250.6	245.3
Night: Vis 0.300-0.400 km	29.4	250.6	250.6	250.6

Similar to the discussion of the SWIR results, this system provides marginal increases in the detection range of the active targets, beyond that of the the visible or PDI systems, but would not provide added value to offshore aviation.

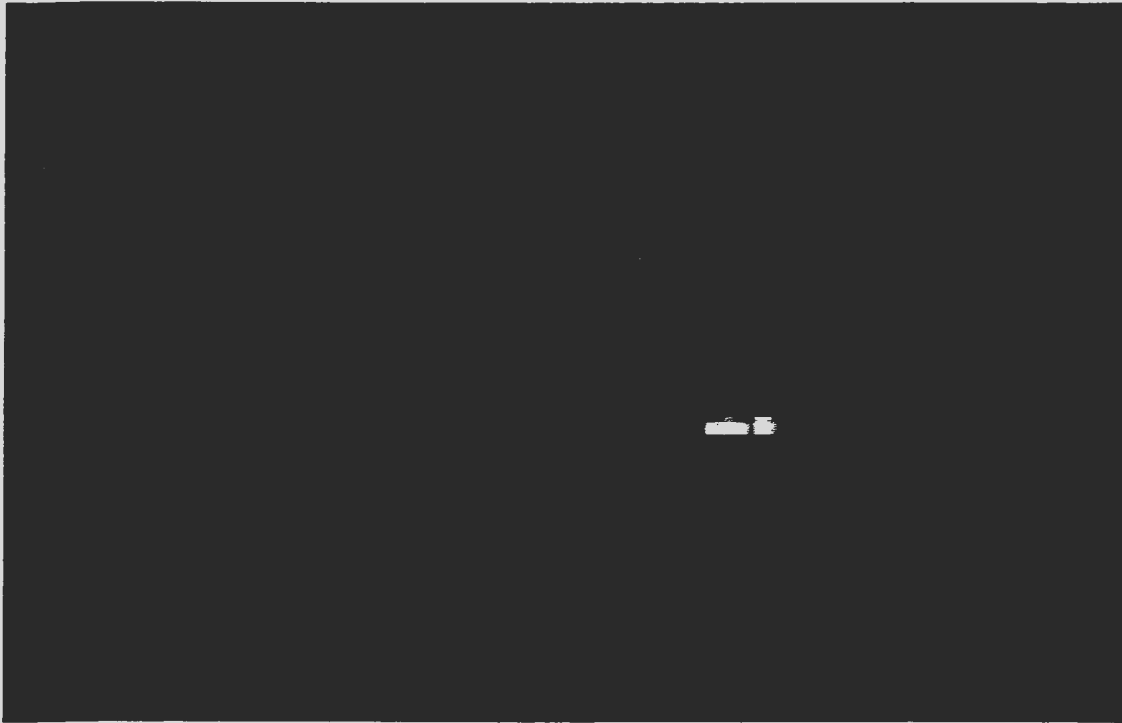


Figure 4.13: 1-5.9 $\mu\text{m}$  image of the targets under moderate daytime fog conditions

#### 4.2.5 Infrared Imaging (3-5 $\mu\text{m}$ )

Images in the 3-5 $\mu\text{m}$  IR region depicted distinct targets under clear daytime, clear nighttime, and foggy nighttime conditions. The imaged targets achieved higher contrasts than other imaging systems, except the PDI system, as illustrated in Tables 4.2 and 4.3. During the 0.250-0.350 km daytime visibility, the 3-5 $\mu\text{m}$  images recorded contrast ratios of 0.114 and 0.130 for the QH sources and 3000W element, respectively. These measurements were substantially lower than those recorded in the SWIR and 1-5.9 $\mu\text{m}$  images. Figure 4.14 depicts 3-5 $\mu\text{m}$  images of the active targets under moderate daytime fog conditions. Intensity measurements are provided in Table 4.10.

Experiments carried out under the moderate daytime fog conditions indicated



Figure 4.14: 3-5 $\mu$ m images of the targets under moderate daytime fog conditions

Table 4.10: 3-5 $\mu$ m target-background intensity measurements

	Background	150W QH	500W QH	3kW Elem
Clear Day	36.7	255.0	255.0	255.0
Clear Night	77.4	255.0	255.0	255.0
Day: Vis 0.250-0.350 km	72.9	81.2	81.2	82.4
Night: Vis 0.300-0.400 km	27.0	251.0	251.0	251.0

that no advantage would be obtained by imaging in the 3-5 $\mu$ m region compared to the visible region.

#### **4.2.6 Infrared Imaging (4-5 $\mu$ m)**

The images captured in the 4-5 $\mu$ m region under both day and night fog conditions presented no useful information. This system, in combination with these targets, performed very poorly under fog conditions and was deemed unsuitable for offshore aviation.

### **4.3 Summary**

This field study found that the polarization difference imaging system achieved the highest contrast ratio in daytime fog conditions. The PDI system's high common mode rejection and inherent target acquisition and tracking features combine to form a system that could provide substantial value to the offshore aviation industry in Newfoundland. The 1-5.9 $\mu$ m system ranked second overall followed by the 1.3-2.5 $\mu$ m system. Comparisons between the 1.3-2.5 $\mu$ m and 1-5.9 $\mu$ m regions, and images in other infrared regions suggest that small advantages can be obtained from imaging in these regions in day fog conditions. Overall, infrared imaging is an expensive alternative that provides no additional benefit to offshore aviation in fog.

Results indicate that the maximum target detection range would be achieved using the 1-2.5 $\mu$ m and 1-5.9 $\mu$ m imaging systems though additional evidence is required to support this claim. The increase in range has not been accurately determined but is known to be small.

Of the enhanced vision systems tested, the PDI system is the only system that would add value to the helicopters flying offshore in fog conditions. The inherent target acquisition and tracking features, high common-mode rejection, simplistic implementation, and low cost would provide the basis for a sophisticated landing aid in fog. A PDI-based system could be used to indicate and maintain lock on the region

**containing the active approach targets. The pilot would search a much narrower field for a visual confirmation of the approach lights. This system would reduce the visual workload, and increase safety and efficiency of flights to offshore oil structures. Chapter 5 discusses a proposed design of a PDI-based target acquisition and tracking system.**

## **Chapter 5**

# **A Polarization Difference Imaging System**

**One fundamental advantage of the polarization difference imaging system over the other systems is its simplicity of image formation and inherent target acquisition and tracking features. The PD image is formed by the subtraction of a horizontally polarized image from a vertically polarized image. A typical scene consisting of primarily unpolarized light, when imaged by a PDI system, would form a very dark image containing very low grayscale values. An active, polarized target or other polarized source would produce a bright region with respect to other unpolarized regions of the scene. The target's location within this scene is detected and differentiated from other sources via a thresholding algorithm.**

**The design of a PD imaging system capable of target acquisition and tracking is an inexpensive, realistic objective. This chapter focuses on a proposed design of such a system in dedicated hardware. The implementation of this design a task left as a future research project in this area.**

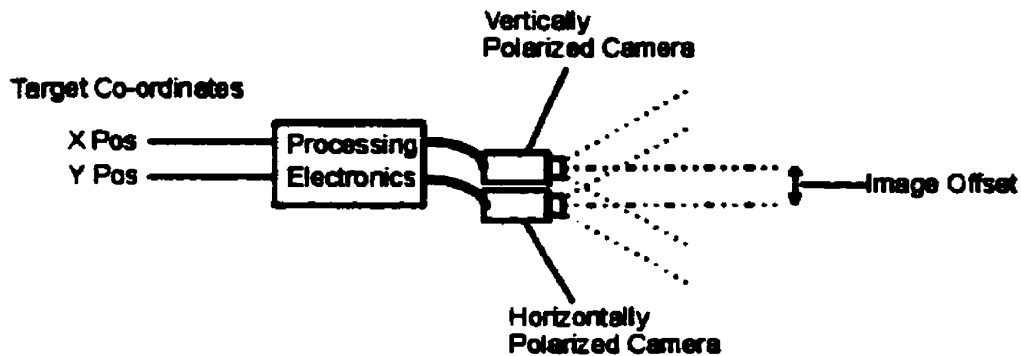


Figure 5.1: Physical setup of the PDI system

## 5.1 Design Overview

The PDI system consists of two cameras mounted side-by-side separated by a small fixed distance. A vertically polarizing filter is mounted over one camera lens while a horizontally polarized lens is mounted over the second camera's lens. The complete imaging system should be mounted on a gimbled platform to ensure optimal alignment between the system and the actively polarized target. A second viable alternative would incorporate a servomechanism to maintain polarization lock. Both registration alternatives permit the system to be used on a moving vehicle. Two standard video streams, in this case RS-170, are transmitted to the processing electronics for target acquisition and tracking. Ultimately, the electronics output X & Y co-ordinates indicating the location of a polarized target within the PD system's field of view. A diagram of the high level setup is presented in figure 5.1.

An spatial offset is present between the vertically and horizontally polarized images due to the physical space occupied by each camera. This offset is removed by clipping the left-most columns in the vertically polarized image and the right-most

columns in the horizontally polarized image. The horizontally polarized image is shifted a fixed amount performing a simple image registration. In a commercial system, image registration could be implemented using a single lens, eliminating the need for the additional electronic processing.

Small misalignment errors are introduced into the PD image after the images are shifted. In order to minimize these errors the separation between the cameras must be small relative to the distance from the scene. In addition, low-pass filtering is performed to reduce sensor noise and to further minimize artifacts and false targets produced by the image shift.

Target detection is performed using a simple thresholding technique. If a region in the PD image exceeds some threshold value, a target has been located and its (X,Y) location is produced at the system output.

The design presented in this chapter is based on camera's using the RS-170 video standard. In order to facilitate an indepth discussion of the PDI system design, it is necessary to briefly discuss the format of the RS-170 video standard.

### **5.1.1 RS-170**

RS-170, as defined by the EIA, is a 525 line, 30 frame per second standard that defines the transmission of a monochrome video signal frequently used in the US. This standard includes definition of synchronization, scan frequency, voltage levels, and blanking timing.

A entire 525 line RS-170 image frame consists of two fields; one field consisting of all the even lines and one field consisting of all the odd lines. Thus each field consists of 262.5 lines, of which 20 lines are used for vertical synchronization leaving 242.5 lines for image information. The grayscale intensity values are encoded in voltage whereas location information is encoded in time.

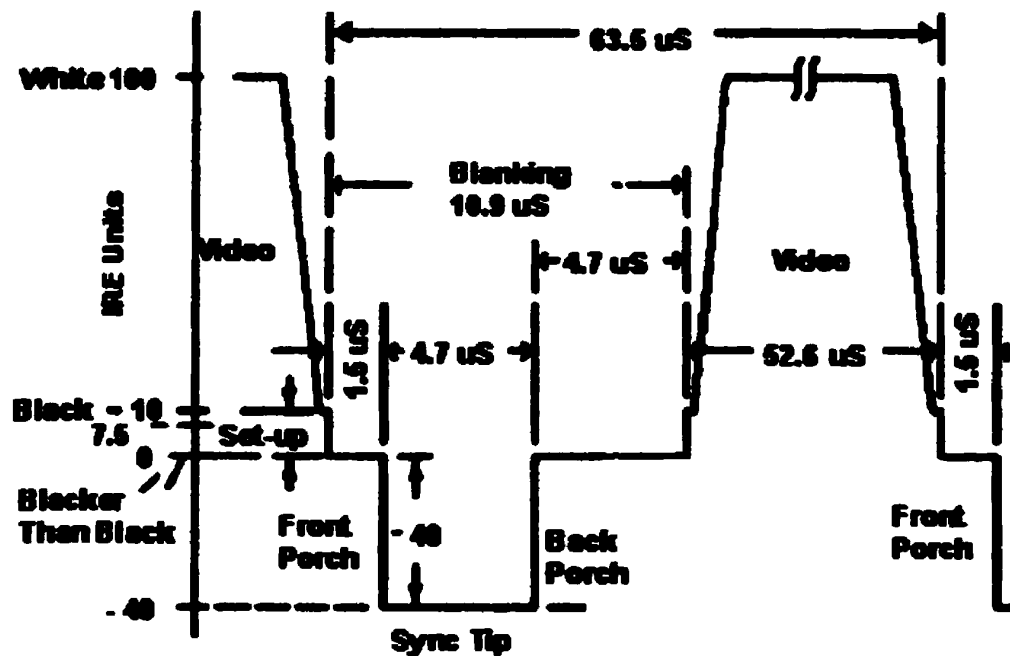


Figure 5.2: Timing diagram of the RS-170 waveform (Modified from [57])

The RS-170 signal has a 1V swing from -0.286 to +0.714V. This range is specified by IRE values with 100 IRE = +0.714V and -40 IRE = -0.286V. Synchronization information is indicated by the 0 IRE to -40 IRE transitions while 0 IRE is the blanking level. Black is represented by 10 IRE while white is represented by 100 IRE. This information, along with the relevant timing information, is illustrated in figure 5.2. The RS-170 standard is well documented in many texts and various informative resources are available on the web.

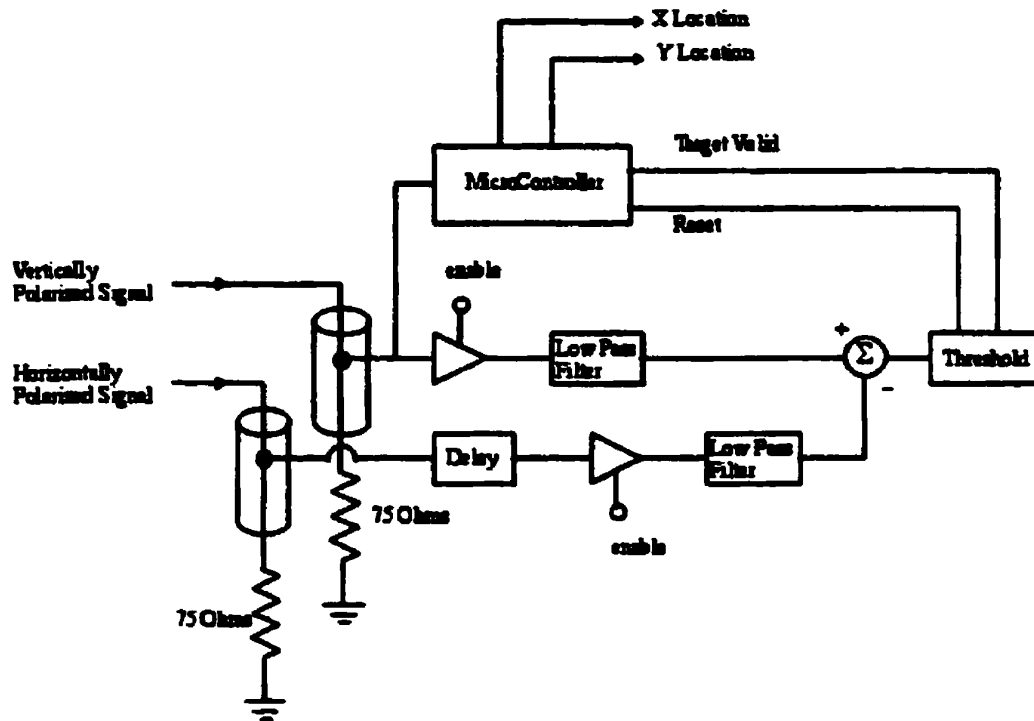


Figure 5.3: Circuit design of the PDI target acquisition and tracking system

## 5.2 PDI Design

The polarization difference imaging system can be designed into dedicated hardware. Figure 5.3 details the high level design of a PDI target acquisition and tracking system.

Both cameras must be synchronized via genlock or other synchronization function available on many systems ensuring that both video signals are aligned in time. The horizontally and vertically polarized video signals are transmitted via  $75\Omega$  co-axial cable and terminated using a  $75\Omega$  resistive load. The  $75\Omega$  load prevents unwanted signal reflections in the co-axial cable.

The horizontally polarized signal delayed to register the images. The delay shifts

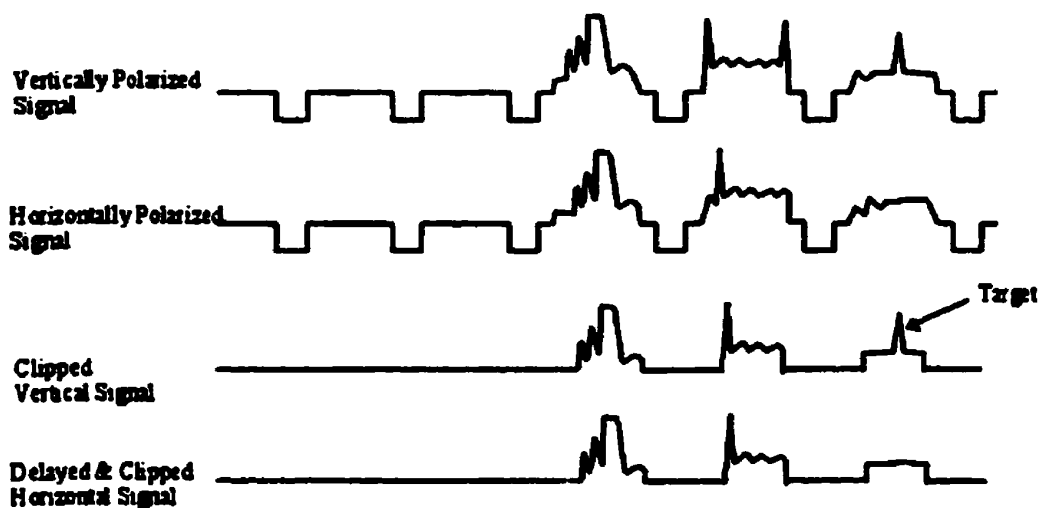


Figure 5.4: Sample vertical and horizontal signals

the horizontally polarized image such that it aligns with the vertically polarized image. A buffer with enable is used to remove synchronization information and non-overlapping video data from the two video signals. The enable signal is generated by the microcontroller when both lines contain valid image information. Each buffer is enabled when both video signals achieve a voltage greater than  $+0.04\text{V}$  or roughly 6 IRE. Samples of both the vertically and horizontally polarized signals and the signals after buffer processing are illustrated in figure 5.4.

The horizontal and vertical polarized signals are low-pass filtered after being edited by the buffer. This filter blurs both images, reducing any image misalignment and eliminating any small false targets.

After filtering, the signals are subtracted to form the difference image and thresholded to detect any targets present. Should the voltage exceed some predefined level, the target valid line is asserted and the microcontroller informed that a target has

been detected. The microprocessor uses the synchronization information to determine the (X,Y) location of the target within the image. The (X,Y) location is output from the PDI system and can be integrated into a complete target acquisition and tracking system.

This discussion presented a potential solution for the PDI target acquisition and tracking system. This system can achieve 30 frames per second and is capable of being implemented without additional processing power. The complete system occupies little space, providing an inexpensive tracking solution to enhance vision through fog.

## **Chapter 6**

# **CONCLUDING REMARKS**

**This work was the first step towards developing research expertise in the field of offshore aviation. The efficiency of helicopter operations on the Grand Banks is well below current industry standards due to the high frequency of dense fog and other adverse meteorological events. Many advanced technologies have been developed, for both military and civilian applications, that could increase the safety and efficiency of offshore aviation operations in inclement weather.**

**In the attempt to initiate research in this field, this thesis examined several enhanced imaging technologies that had potential to improve helicopter flights on the Grand Banks. A thorough review of the literature provided details on the cutting-edge research being conducted worldwide. Scientists and researchers have examined vision systems ranging from laser-based imagers to imaging millimeter-wave radiometers in the hopes of allowing flights into zero visibility conditions.**

**It was evident from the literature that little field work had been completed in a marine environment as severe as that found in Newfoundland. Several companies interested in having their products tested in this environment sent prototypes for a two week evaluation period. Two infrared cameras, along with an assortment of**

lenses, were obtained and prepared for the vision trials conducted at Cape Race, Newfoundland.

Before the trials began, it was necessary to develop a visibility sensor capable of quantifying the baseline visibility. A camera-based sensor was designed and tested over a two month period. This sensor, which relied on the fundamental visibility theory, demonstrated excellent accuracy when compared to commercial visibility sensors employed at the St. John's International Airport. The visibility sensor, along with various other meteorological instruments were used to measure baseline performance of the various enhanced imaging solutions.

The enhanced vision field trials examined visible, polarization difference, and several infrared imaging systems to determine the advantages and disadvantages of each system when imaging active targets through fog. Polarization difference imaging performed quite well during the field trials, producing distinct target images in visibilities down to 0.250 km. This system demonstrated excellent target acquisition and tracking characteristics capable of acquiring and tracking the landing lights under various day fog conditions. It provided the basis for a enhanced vision solution designed to track the approach lights of an offshore structure in fog, providing pilots with a small region in which the approach aids are found. The PDI system was the only enhanced vision solution examined that would provide value to commercial operations offshore.

A PDI-based target acquisition and tracking system is proposed in Chapter 5 as a potential dedicated hardware solution. Implementation of this solution is left as future work.

## **6.1 Future Work**

This research investigated potential approaches to enhancing vision for improved offshore aviation in visibility conditions. As with any research project, there is always

additional work to be done in many areas.

The field trials conducted at Cape Race were limited to a two week period as the cameras had to be returned to the companies. Additional testing is needed to support the findings of these investigations and confirm the results of imaging in the 1-2.5 $\mu\text{m}$  and 1-5.9 $\mu\text{m}$  regions. These tests should include instruments capable of measuring more specific fog characteristics such as liquid water content and droplet size distribution. These measurements would provide a better source of baseline data on the fog events and better indicators of infrared performance in fog. Unfortunately, this equipment was not available during the course of this project.

The next logical extension of this research project would include construction of the PDI-based target acquisition and tracking system proposed in Chapter 5. This system should be integrated into a complete heads-up display solution suitable for additional trials involving human subjects. Human performance in target acquisition and tracking in various day fog conditions with and without the PDI system would support further development of this system.

# References

- [1] R. E. Huschke, *Glossary of Meteorology*, AMS, Boston, 1959.
- [2] W. E. Middleton, *Vision Through The Atmosphere*, University of Toronto Press, Canada, 1958.
- [3] <http://www.offshore-technology.com/projects/hibernia>.
- [4] D. McFarlan, *The Guinness Book of Records 1990*, Guinness Publishing Ltd., 1989.
- [5] H. Smith, "Effectively Operating in Harsh Environments Can Add Significant Value", *Proceedings of Second Workshop on Offshore Aviation Research*, C-CORE Publication 98-33, 1998.
- [6] K. Jamieson, "Development of Practical Offshore GPS Instrument Approaches and Lighting Systems", *Proceedings of Second Workshop on Offshore Aviation Research*, C-CORE Publication 98-33, 1998.
- [7] L. E. Mertens, *In-Water Photography*, Wiley-Interscience, New York, 1970.
- [8] M. G. Heaps, "Vertical structure of aerosols within boundary layer for low-visibility/low-stratus conditions" *Hygroscopic Aerosols*, L.H. Ruhnke and A. Deepaks eds., A. Deepak Publishing, Hampton, Virginia, 1984, pp.69-91.

- [9] H. Koschmieder, "Theorie der horizontalen Sichtweite" *Beitr. Phys. freien Atm.*, 12:33-53;171-181.
- [10] G. Tonna and K. S. Shifrin, "Reliability of the polar nephelometer for the measurement of visibility in fog" *Applied Optics*, 31, 1992, 2932-2941.
- [11] C. S. Mill, D. Lacey, and M. J. Gay, "A novel device to measure atmospheric visibility" *Measurement Science Technology*, 5, 1994, pp.1505-1512.
- [12] J. Bendix, "Determination of fog horizontal visibility by means of NOAA-AVHRR" *Int. J. Remote Sensing*, 1995, pp.1847-1849.
- [13] D. Pomerleau, "Visibility Estimation from a moving Vehicle using the Ralph Vision System" *IEEE conference on Intelligent Transportation Systems*, Boston, Mass., 1997, pp.906-911.
- [14] C. Busch and E. Debes, "Wavelet Transform for Analyzing Fog Visibility" *IEEE Intelligent Systems*, 1998, pp.66-71.
- [15] L. Bissonnette, G. R. Roy, C. Bastille, and G. Vallée "Visibility of lighting systems in fog" C-CORE 96-C14, Newfoundland, 1996.
- [16] K. Klein "A Method for Evaluating Commercial Helideck Lighting Product Performance in Fog" C-CORE 96-C41, Newfoundland, 1996.
- [17] J. Gordon, "Daytime visibility: a conceptual review," AFGL-TR-79-0257, Phillips Laboratory, Hanscom, MA, 1979.
- [18] L. Wilk, <http://www.reefnet.on.ca/gearbag/wwwlux.html>, 1996.
- [19] T.S. Lomheim, "Introduction to Color Imaging Using CCDs and Solid State Sensors," SPIE, Bellingham, WA, 1996.

- [20] Gonzales and Wintz, *Digital Image Processing*, Addison-Wesley, 1977.
- [21] S. Valley, *Handbook of Geophysics and Space Environments*, McGraw-Hill, New York, 1965.
- [22] S. A. Clough, F. K. Kneizys, L. S. Rothman, and W. O. Gallery, *Atmospheric Transmittance and Radiance: FASCODIB*, TR-81-0269, Air Force Geophysics Laboratory, Hanscom, MA, 1981.
- [23] P. Klass, "Forward-Scatter' RVR Aims to Cut Weather Delays" *Aviation Week & Space Technology*, January 22, 1998, pp.39-40.
- [24] N. S. Kopeika, "Effects of aerosols on imaging through the atmosphere: a review of spatial frequency and wavelength dependent effects" *Optical Engineering*, 24(4), 1985, pp.707-712.
- [25] L. R. Bissonnette, "Calculation method of the modulation transfer function in aerosol media" *Propagation Engineering*, Proceedings of SPIE, v.1312, 1990.
- [26] L. R. Bissonnette, "Blurring effect of aerosols on imaging systems" *Propagation Engineering*, Proceedings of SPIE, v.1487, 1991.
- [27] L. R. Bissonnette, "Imaging through fog and rain" *Optical Engineering*, 31(5), 1992, pp.1045-1052.
- [28] J. R. Linskens, and C. F. Bohren, "Appearance of the Sun and the Moon through clouds" *Applied Optics*, 33(21), 1994, pp.4733-4740.
- [29] J. P. Oakley, B. L. Satherly, C. G. Harrison, and C. S. Kydeas "Enhancement of image sequences from a forward-looking airborne camera" *Image and Video Processing IV*, Proceedings of SPIE, v.2666, 1996.

- [30] J. P. Oakley, and B. L. Satherly, "Improving Image Quality in Poor Visibility Conditions Using a Physical Model for Contrast Degradation" *IEEE Transactions on Image Processing*, 7(2), 1998, 167-179.
- [31] N. Engheta, J. S. Tyo, M. P. Rowe, and E. N. Pugh, Jr., "Biologically Inspired Polarization Difference Imaging" *European Microwave Conference and Exhibition 97*, IEEE, 1997, 978-983.
- [32] J. S. Tyo, "Polarization Difference Imaging: A Means for seeing through Scattering Media" Doctoral Thesis, University of Pennsylvania, 1997.
- [33] B. D. Nordwall, "Navy Tests Lasers To Help Carrier Pilots" *Aviation Week & Space Technology*, Nov. 19, 1990, 46-48.
- [34] B. MacDonald, "Report on Laser Approach Lighting Trial" Cougar Helicopters Inc., St. John's, NF, 1997.
- [35] R. B. Lumsden and A. J. Smith, "A Review of Recent UK Research in Support of Offshore Aviation" *Proceedings of Second Workshop on Offshore Aviation Research*, C-CORE Publication 98-33, 1998.
- [36] L. R. Bissonnette, "Visibility of lighting systems in fog" Defence Research Establishment Valcartier, 1996.
- [37] D. Hart, G. Piercey, N. Hansen, S. Smyth, D. Christian, and P. Kumar, "Baseline Data from the Torbay Precipitation Facility" *Proceedings of Second Workshop on Offshore Aviation Research*, C-CORE Publication 98-33, 1998.
- [38] J. Nordwall, M. Pavel, A. Ahumada, and B. Sweet, "Engineering a Visual System for Seeing Through Fog" *22nd International Conference on Environmental Systems*, SAE, 1992.

- [39] unlisted, "Helping Pilots See Through the 'Soup'" *NASA Facts*, National Aeronautics and Space Administration, 1993.
- [40] M. K. Kaiser, and J. P. Jenkins, "Enhanced/Synthetic Vision Systems for Advanced Flight Decks"  
<http://olias.arc.nasa.gov/publications/kaiser/sid94/sid94.html>, 1993.
- [41] B. T. Sweet, and C. Tiana, "Image processing and fusion for landing guidance" *Enhanced and Synthetic Vision 1996*, SPIE, v. 2736, 1996, 84-95.
- [42] unlisted, "'Enhanced Vision' Goal: Fly Anywhere, Anytime" *Aviation Week & Space Technology*, Apr. 21, 1997, 53.
- [43] K. Beier, R. Bhl, J. Fries, W. Hahn, D. Hausamann, V. Tank, G. Wagner, and H. Weisser, "Measurement and modelling of infrared imaging systems at conditions of reduced visibility (fog) for traffic applications", SPIE, v. 2223, 1994, 175-186.
- [44] L. J. Denes, R. Grace, D. A. Purta, and A. M. Guzman, "Assessment of driver vision enhancement technologies" *Collision avoidance and automated traffic management sensors*, SPIE, v. 2592, 1995, 17-28.
- [45] R. N. Lane, "The SWIR Advantage" *Airborne Reconnaissance XIX*, SPIE, v. 2555, 1996, 246-254.
- [46] C. A. MacCarley, B. Hemme, and L. Klein, "An Assessment of Infrared and Millimeter-wave Imaging For Traffic Surveillance and Detection", Transportation Electronics Institute, California Polytechnic State University, 1998.
- [47] W. F. Horne, S. Ekiert, J. Radke, R. R. Tucker, C. H. Hannan, and J. A. Zak, "Synthetic Vision System Technology Demonstration Methodology and Results to Date" *Aerospace Technology Conference and Exposition*, Aerotech, 1992.

- [48] T. W. Bradley, M. W. Autry, and L. H. Hui, "MMW technology For Enhanced Situation Awareness/Enhanced Vision Systems" *IEEE National Telesystems Conference*, IEEE, 1993, 97-99.
- [49] J. Lovberg, R. Chou, and C. Martin, "Real-time Millimeter-Wave Imaging Radiometer for Avionic Synthetic Vision" *Sensing, Imaging, and Vision for Control and Guidance of Aerospace Vehicles*, SPIE, 2220, 1994, 234-244.
- [50] M. Shoucri, G. S. Dow, B. Hauss, P. Lee, and L. Yujiri, "Passive Millimeter Wave Camera for Vehicle Guidance in Low Visibility Conditions" *Synthetic Vision for Vehicle Guidance and Control*, SPIE, 2463, 1995, 2-9.
- [51] L. Yujiri, H. Agravante, et. al., "Passive millimeter-wave camera" *Passive Millimeter-Wave Imaging Technology*, SPIE, 3064, 1997, 15-22.
- [52] S. Fornaca, M. Shoucri, and L. Yujiri, "Passive millimeter-wave video camera for aviation applications" *Enhanced and Synthetic Vision 1998*, SPIE, 3364, 1998, 20-25.
- [53] D. Bonnier, and V. Larochelle, "A range-gated active imaging system for search and rescue, and surveillance operations", Defence Research Establishment Valcartier, 1998.
- [54] V. Larochelle, D. Bonnier, G. Roy, J. Simard, and P. Mathieu, "Performance assessment of various imaging sensors in fog", *Enhanced and Synthetic Vision 1998*, SPIE, v. 3364, 1998, 66-80.
- [55] S. G. Owen,  
<http://www.css.tayloru.edu/instrmat/graphics/hypervis/vistoc.htm>, 1997.
- [56] K. Matkovic, <http://www.cg.tuwien.ac.at/research/theses/matkovic/>, 1997.

[57] <http://www.ntsc-tv.com/ntsc-index-02.htm>, 1998.

[58] P. Kumar, "Briefing Note", *Proceedings of the First Workshop on Offshore Aviation Research*, C-CORE, 1997.







